Repair-independent functions of DNA-PKcs protect irradiated cells from mitotic slippage and accelerated senescence

Yue Liu, Elena V. Efimova, Aishwarya Ramamurthy & Stephen J. Kron*

Department of Molecular Genetics and Cell Biology and Ludwig Center for Metastasis Research, The University of Chicago, 929 East 57th Street, Chicago, IL, 60637

*Corresponding author:

Phone: 773-834-0250

skron@uchicago.edu

Keywords:

DNA-PKcs, DNA damage response, ATM, mitotic slippage, senescence

Summary statement:

Though unnecessary for non-homologous end joining in irradiated cells, DNA-PKcs serves a critical role after DNA repair by downregulating DNA damage signaling, protecting cells from mitotic slippage and accelerated senescence.

JCS Advance Online Article. Posted on 12 June 2019

Abstract

The binding of DNA-dependent protein kinase catalytic subunit (DNA-PKcs) to Ku proteins at DNA double strand breaks (DSBs) has long been considered essential for non-homologous end joining (NHEJ) repair, providing a rationale for DNA-PKcs inhibitors as cancer therapeutics. Given lagging clinical translation, we reexamined mechanisms and observed instead that DSB repair can proceed independently of DNA-PKcs. While repair of radiation-induced DSBs was blocked in cells expressing shRNAs targeting Ku proteins or other NHEJ core factors, DSBs were repaired on schedule despite targeting DNA-PKcs. Although we failed to observe a DSB repair defect, γH2AX foci persisted indefinitely after irradiation, leading to cytokinesis failure and accumulation of binucleated cells. Following this mitotic slippage, cells with decreased DNA-PKcs underwent accelerated senescence. We identified down-regulation of ataxia-telangiectasia mutated kinase (ATM) as the critical role for DNA-PKcs in recovery from DNA damage insofar as targeting ATM restored γH2AX foci resolution and cytokinesis. Considering the lack of direct impact on DSB repair and emerging links between senescence and therapy resistance, these results suggest reassessing DNA-PKcs as a cancer target.

Introduction

When cancer cells are subjected to genotoxic stress, failure to detect or repair DNA double strand breaks (DSBs) may result in mitotic catastrophe or lethal aneuploidy, leading to the presumed benefits of radiation and chemotherapy (Ciccia and Elledge, 2010). A common rationale for targeting the DNA damage response (DDR) in cancer is to potentiate genotoxic therapy by blocking checkpoint arrest and repair (O'Connor, 2015). Of the 500-some proteins that mediate the DDR (Pearl et al., 2015), the DNA-dependent protein kinase catalytic subunit (DNA-PKcs, PRKDC, XRCC7) is considered a central player in DNA damage signaling and DSB repair. An early event at many DSBs is the binding of the Ku70 and Ku80 proteins which can recruit DNA-PKcs and initiate repair via the conventional Ligase 4-dependent non-homologous end joining (NHEJ) pathway (Jette and Lees-Miller, 2015) . The logic that targeting NHEJ may confer or restore sensitivity to therapy has led to substantial efforts to develop DNA-PKcs inhibitors as cancer drugs (Davidson et al., 2013; Salles et al., 2006). Though several clinical candidates remain under study, others have been abandoned during development and none have reached the clinic.

DNA-PKcs and ataxia-telangiectasia mutated kinase (ATM) (Yang et al., 2003) are closely related members of the phosphatidylinositol 3-kinase-related kinase (PIKK) superfamily with shared functions in the DDR, including phosphorylating Ser139 in the carboxyl terminal tail of histone H2AX in nucleosomes adjacent to DSBs, forming γH2AX foci (Stiff et al., 2004). DNA-PKcs and ATM also phosphorylate each other (Chen et al., 2007), with DNA-PKcs serving as a negative regulator of ATM (Finzel et al., 2016; Zhou et al., 2017). This negative feedback may explain the seemingly inconsistent observations that while ATM inhibitors block γH2AX foci formation (Burma et al., 2001) and suppress checkpoint arrest and cellular senescence (Kang et al., 2017), DNA-PK inhibitors delay γH2AX foci resolution and promote checkpoint arrest and cellular senescence (Azad et al., 2011; Ciszewski et al., 2014; Sunada et al., 2016; Zhao et al., 2006).

A complementary concern is that cell lines deficient for DNA-PKcs often display reduced ATM expression (Neal and Meek, 2019). Though mechanisms have yet to be fully defined, the effect can be recapitulated by siRNA knockdown of DNA-PKcs (Peng et al., 2005) and has been linked to overexpression of microRNA miR-

100 in DNA-PKcs$^{-/-}$ cells (Ng et al., 2010). Nonetheless, while the most parsimonious explanation for the DNA repair defects and radiation sensitivity in DNA-PKcs deficient cells is their lack of DNA-PKcs activity, this fails to account for the confounding effects of ATM downregulation, which may suppress all aspects of the DNA damage response including DSB repair.

Using MCF7 breast cancer as a model, we observed that specifically inhibiting DNA-PKcs conferred the expected increase in sensitivity to radiation, but this was not linked to a DSB repair defect. As with chemical inhibition, partial knockdown of DNA-PKcs allowed DSBs to be repaired without delay. Despite apparently having completed repair, the γH2AX foci formed at chromosomal breaks failed to resolve, indicating a persistent DDR. When these cells progressed to mitosis, they displayed high rates of cytokinesis failure. The surviving binucleate cells adopted the characteristic senescent phenotype of flattened cell shape and expression of senescence-associated β-galactosidase (SA-βGal). By contrast, knockdown of the Ku proteins or other core NHEJ factors was able to block DSB repair but γH2AX foci resolved on schedule, followed promptly by cell division resulting in mitotic catastrophe.

Prior studies have linked DNA-PKcs inhibition to defects in mitosis, potentially mediated by loss of interactions with polo-like kinase 1 (PLK1) and/or phosphatase 6 (PP6) (Douglas et al., 2014). However, we find that the persistent γH2AX, mitotic slippage and accelerated senescence after irradiation of cells with decreased DNA-PKcs activity could all be suppressed by subsequent inhibition of ATM. Thus, while DNA-PKcs clearly plays a key role in regulating DNA damage response, our data unlink DNA-PKcs from NHEJ repair and instead define a new role in protecting cells from persistent ATM-dependent DNA damage signaling. Although blocking DNA-PKcs can inhibit proliferation after irradiation, cells remain viable after undergoing therapy-induced senescence. Given recent studies suggesting reversibility of senescence (Chakradeo et al., 2016; Wang et al., 2013) and implicating senescent tumor cells in cancer recurrence after therapy (Demaria et al., 2016), our results suggest reevaluating the rationale for clinical development of DNA-PKcs inhibitors.

Results

Inhibition of DNA-PKcs induces persistent γH2AX, enhances radiosensitivity and accelerates cellular senescence

Toward reexamining DNA-PKcs functions in the DNA damage response (DDR) following exposure to ionizing radiation (IR), we inhibited DNA-PKcs in MCF7 cells and then irradiated the cells to induce double strand breaks (DSBs). DNA-PKcs was targeted by transducing MCF7 cells with lentivirus expressing short hairpin RNA (shRNA) to target DNA-PKcs transcripts (shDNA-PKcs, Fig. S1A) or treating cells expressing a scrambled shRNA control (shScr) with Nu7026 (2-(morpholin-4-yl)-benzo-[h]chomen-4-one (Nutley et al., 2005)), a potent DNA-PKcs kinase inhibitor with >100 fold selectivity over ATM. We monitored the dynamics of IR-induced chromatin foci (IRIF) by immunofluorescence (IF) to detect the phosphorylation of histone H2AX to form γH2AX foci and localization of 53BP1, an adapter protein that binds at DSBs to promote DNA damage signaling and promote end-joining over homologous recombination (Panier and Boulton, 2014). As expected for irradiated controls (Rogakou et al., 1998; Schultz et al., 2000), IF analysis of shScr at 0.5 h after irradiation revealed γH2AX and 53BP1 colocalized at multiple nuclear foci that decreased in number by 2 h and largely resolved within 24 h (Fig. 1A, C), presumably reflecting the kinetics of normal DSB detection and repair. Consistent with prior studies (Bouquet et al., 2006), the few foci remaining at 24 h were larger and brighter, indicating spreading of γH2AX across chromatin near unrepaired single or clustered DSBs. Further, as expected, shDNA-PKcs or shScr treated with Nu7026 each formed γH2AX and 53BP1 foci by 0.5 h, but they failed to resolve by 24 h, suggesting persistent DSBs (Fig. 1B, C). In agreement with IF results, Western blotting revealed similar γH2AX immunoreactivity at 0.5 and 2 h after radiation with or without Nu7026, but persistent γH2AX at 24 h with Nu7026 (Fig. 1D, S1B and S1C). The rapid activation of DNA-PKcs in control cells detected by Thr2609 phosphorylation and Ser2056 phosphorylation (p-DNA-PKcs) was suppressed by Nu7026 (Fig. 1D, S1and S1C).

Consistent with the high γH2AX levels that remained in shDNA-PKcs or Nu7026-treated shScr after irradiation, clonogenic assays revealed a decreased surviving fraction in shDNA-PKcs cells or shScr treated with Nu7026 (Fig. 1E). Live-

cell time-lapse imaging and automated cell proliferation analysis of shScr cells responding to 6 Gy in the presence or absence of Nu7026 showed that while control cells recovered within 1 day, Nu7026 suppressed cell division for up to 7 days (Fig. 1F). Given that inhibiting DNA-PKcs promotes cellular senescence (Azad et al., 2011), we examined the shScr cells after five days, finding that DNA-PKcs inhibition increased the fraction of enlarged cells with flattened morphology expressing SA-βGal (Fig. 1G).

Persistent γH2AX is independent of DSB repair

Reflecting the critical role attributed to DNA-PKcs in conventional NHEJ throughout the cell cycle (Chang et al., 2017) (Fig. 2A), γH2AX foci persistence after DNA-PKcs inhibition is typically ascribed to unrepaired DSBs. To evaluate DSB repair after blocking conventional NHEJ, we constructed shXRCC6 and shXRCC5 lines to knock down the Ku70/Ku80 heterodimer and DNA-PKcs recruitment as well as shXLF, shXRCC4, shPAXX, and shLig4 to target NHEJ factors downstream of DNA-PKcs (Fig. S1A). Neutral comet assays confirmed that shRNA targeting conventional NHEJ factors (shNHEJ) significantly increased levels of unrepaired DSBs at 24 h (Fig. 2B). Irrespective of the different repair defects in each shNHEJ cell line, Nu7026 failed to increase residual damage. Like shScr, each of the shNHEJ cell lines formed γH2AX foci by 2 h (Fig. S2) that resolved by 24 h (Fig. 2C, E). In turn, treating shScr or shNHEJ cells with Nu7026 induced foci persistence (Fig. 2D, E).

Taken together, these data indicate that γH2AX foci formation may depend on DNA damage but not DNA-PKcs, while foci resolution depends on DNA-PKcs but not DNA repair. To directly examine DSB repair in the absence of DNA-PKcs, shScr and shDNA-PKcs, with or without Nu7026, were irradiated and neutral comet assays performed after 24 h, revealing similar levels of residual DBSs (Fig. 2F). A time course in shScr cells showed *less* damage at 2 h after treatment with Nu7026 and a similar return to baseline by 24 h (Fig. 2G). A second potent and selective DNA-PKcs inhibitor, Nu7441 (8-dibenzothiophen-4-yl-2-morpholin-4-yl-chromen-4-one (Leahy et al., 2004)), recapitulated Nu7026's effects on MCF7 cells (Fig. S3A, B and C). As with MCF7, Nu7026 similarly blocked foci resolution without inhibiting DSB repair in multiple cell lines including MDA-MB-435, MDA-MB-231, B16-F10, and CT26 (Fig. S3G - K).

When conventional NHEJ fails, alternative end joining (altEJ) (Iliakis, 2009; Lieber, 2010) can complete DSB repair, a potential mechanism to compensate for DNA-PKcs inhibition. Thus, MCF7 cells were developed expressing shRNAs to knock down the altEJ factors XRCC1 or Lig3 (Iliakis, 2009) (Fig. S1A). Much like in shScr or shNHEJ, foci formed and resolved in the altEJ shRNA cells on schedule but persisted upon treatment with Nu7026 (Fig. S4A-D). In turn, the minor DSB repair defect in shXRCC1 and shLig3 was not enhanced by Nu7026 (Fig. S4E), arguing against activation of altEJ upon DNA-PKcs inhibition.

ATM activity maintains γH2AX persistence

ATM has long been considered to serve a unique role in the DDR (Yang et al., 2003). Upon activation by DSBs (Hartlerode et al., 2015; You et al., 2007), ATM mediates phosphorylation of H2AX in proximal nucleosomes (Burma et al., 2001), leading to 53BP1 accumulation and foci formation. ATM also recruits NHEJ factors to stimulate repair (Blackford and Jackson, 2017). Recent reports (Finzel et al., 2016; Zhou et al., 2017) of negative regulation of ATM by DNA-PKcs raise the question whether DNA-PKcs inhibition phenotypes can be explained mechanistically by ATM deregulation. Thus, we used MCF7$^{GFP\text{-}IBD}$ cells expressing GFP fused to the 53BP1-IRIF binding domain (IBD) (Efimova et al., 2010) as a live-cell reporter to examine the relative contributions of DNA-PKcs and ATM to foci formation and persistence (Fig. 3A). Consistent with the IF analysis, Nu7026 did not appreciably alter GFP-IBD foci numbers at 2 h but blocked foci resolution at 24 h (Fig. 3B). The selective ATM inhibitor Ku55933 (2-(4-morpholinyl)-6-(1-thianthrenyl)-4*H*-pyran-4-one (Hickson et al., 2004)), alone or combined with Nu7026, blocked foci formation. To examine a role for ATM in foci persistence, we applied the inhibitors in sequence (Fig. 3C). MCF7$^{GFP\text{-}IBD}$ was treated with either Nu7026 or Ku55933 starting 1 h before irradiation and until 24 h after IR. Cells were then washed and incubated with either Nu7026 or Ku55933 for an additional 24 h and foci were compared to DMSO control (Fig. 3D). Cells treated with only Nu7026 or Ku55933 displayed foci persistence and lack of foci formation, respectively. However, persistent foci induced by Nu7026 resolved upon transfer to Ku55933. To distinguish among potential mechanisms, we examined the dynamics of GFP-IBD in single foci by fluorescence recovery after photobleach (FRAP) analysis (Fig. S5A and B). GFP-IBD remained nearly as dynamic at 24 h as 30 min, whether cells were treated with DMSO or

Nu7026. Taken together, these data suggest that foci persist as long at ATM remains active, perhaps reflecting a requirement for ATM to maintain γH2AX.

DNA-PKcs downregulates ATM activity to suppress the DDR

To further examine order of function between DNA-PKcs and ATM, we established MCF7 cells expressing shRNA targeting ATM (Fig. S1A). Additionally, we stabilized activated DNA-PKcs in MCF7 cells via shRNA targeting RNF144A, an E3 ubiquitin ligase purported to promote DNA-PKcs degradation (Ho et al., 2014) (Fig. 4A ,S5C, and S5D). shRNF144A induced persistent p-DNA-PKcs (S2056) at 24 h after IR and induced the loss of p-ATM (S1981) across the time course but had only minor if any impact on the total amounts of DNA-PKcs or ATM (Fig. S5D). Neutral comet assays revealed similar DSB repair defects in shRNF-144A and shATM cells (Fig. 4B). Strikingly, inhibition of DNA-PKcs with Nu7026 suppressed the DSB repair defect not only in shRNA-144A cells but in shATM cells. The latter effect may reflect reactivation of the remaining ATM protein expressed by shATM cells.

These results raised the question of how shATM and shRNA-144A might affect foci formation and resolution. Compared to shScr, irradiation of shATM generated fewer γH2AX and 53BP1 foci at 0.5 or 2 h (Fig. 4C). These residual foci were lost upon treatment with Nu7026, consistent with previous observations that DNA-PKcs can initiate γH2AX foci formation in ATM-deficient cells (Stiff et al., 2004). By 24 h, the foci in shATM cells resolved (Fig. 4C, E). shRNF-144A, with or without Nu7026, displayed similar foci kinetics to shScr (Fig. 4D, E). Together, these results support an on-off mechanism whereby ATM, activated upon sensing damage, feeds forward to stimulate DNA-PKcs and enhance detection of DSBs but then once repair is complete, the active DNA-PKcs feeds back to downregulate ATM.

Several prior studies have observed γH2AX and/or 53BP1 foci in the absence of DSBs. Persistent foci, whether associated with damage or not, are associated with cellular senescence (Fumagalli et al., 2014; Rodier et al., 2009). However, shNHEJ cells, though lacking persistent foci, displayed enhanced senescence compared to shScr (Fig. 5A, B), supporting a direct role for persistent DSBs in senescence. That treating shNHEJ cells with Nu7026 further increased the percentage of senescent cells (Fig. 5A, B) suggests independent contributions of DSBs and foci to signaling, though each may require ATM to have its effects.

DNA-PKcs protects against accelerated senescence by promoting cytokinesis

Along with DSB repair defects, DNA-PKcs inhibition has been associated with prolonged checkpoint arrest as well as mitotic defects leading to failed cytokinesis (Shang et al., 2010), resulting in mononucleated or binucleate tetraploid cells that progress into senescence (De Santis Puzzonia et al., 2016). To examine mitotic progression after irradiation, MCF7 cells were treated with 0 or 6 Gy, with or without Nu7026, incubated 24 h, immunostained for γH2AX, counterstained with DAPI and analyzed by flow cytometry. In unirradiated cells, Nu7026 appeared to suppress S phase, increasing the proportions of 2N (presumptive G1) and 4N (presumptive G2/M) cells (Fig. S6A). After irradiation, control cells displayed increased γH2AX, accumulation in G1 and decreased S and G2/M fractions (Fig. 6A). Nu7026 led to a further increase in γH2AX and an apparent shift toward 4N DNA content, consistent with a prolonged G2/M DNA damage checkpoint arrest or mitotic slippage. Thus, we applied live-cell time-lapse imaging to track cell cycle progression in MCF7 cells expressing FUCCI (Sakaue-Sawano et al., 2008) fluorescent cell cycle reporters, where G1 cells express mCherry-hCdt1 (red) and S/G2 cells express mVenus-hGeminin (green). Early in S phase, cells express both reporters and between M and G1, they express neither (Fig. 6B). Nu7026 had no appreciable effects on mitosis or cytokinesis in unirradiated cells (Fig. S6B, Movie S1). However, Nu7026-treated irradiated cells displayed mitotic slippage, appearing to enter mitosis (green), round up, and initiate cytokinesis but due to a cytoplasmic bridge, nascent daughter cells (red) collapsed together to generate binucleate cells that adopted a flattened morphology characteristic of senescence (Fig. 6B, Movie S1). Blocking ATM with Ku55944 partially rescued cells from cytokinesis defects and cellular senescence driven by DNA-PKcs deficiency (Fig. S6C, Movie S2).

While shDNA-PKcs and shLig4 each promoted senescence after irradiation, they displayed distinct patterns of DSB repair and foci persistence. To examine if they follow distinct pathways to senescence, we used live-cell time-lapse imaging to record shScr, shDNA-PKcs and shLig4 cells after irradiation in the presence or absence of Nu7026. For each condition, we tracked the trajectories of twenty cells through one or more rounds of cell division to determine if they yielded independent daughter cells (Fig. 6C) and assembled their trajectories over time (Fig. 6D, Fig. S6C). Here, to indicate abortive cytokinesis, nascent daughter cells were counted as two cells even if they remained connected by a cytoplasmic bridge. While shDNA-

PKcs cells displayed cytokinesis failure and accumulated as binucleated cells, shLig4 returned to cell division within a day, presumably undergoing mitotic catastrophe. When shScr, shLig4 and shDNA-PKcs cells were treated with Nu7026 and then irradiated, all three displayed cytokinetic failure. We also examined the accumulation of flat, SA-βGal positive senescent cells at 4 days after irradiation, noting the fraction that appeared mononucleate or binucleate (Fig. 6E). Although shLig4 displayed increased SA-βGal positive cells after 6 Gy, the majority of these senescent cells were mononucleated. Together with the flow cytometry analysis, this suggests senescence in shLig4 may reflect an irreversible cell cycle arrest prior to onset of S phase rather than after mitotic slippage.

To confirm a mechanism linking mitotic slippage to senescence via formation of binucleated cells, even without prior DNA damage (Panopoulos et al., 2014), we treated MCF7 FUCCI cells with the small molecule kinase inhibitors AZD1152-HQPA (barasertib) and GSK461364 to target Aurora B or PLK1 respectively and thereby disrupt mitosis and/or cytokinesis (Fededa and Gerlich, 2012). Time-lapse imaging confirmed each inhibitor conferred a cytokinesis defect in unirradiated cells much like that observed with DNA-PKcs inhibition in irradiated cells, leading to binucleate cells that flattened out to adopt a senescent cell phenotype (Fig. S6E, Movie S3). In turn, staining analysis after 4 days treatment with the kinase inhibitors revealed increased SA-βGal, with a high proportion of binucleate senescent cells (Fig. S6E - G). A caveat is that most binucleate cells formed after Aurora B and PLK1 inhibition died rather than entering senescence (Fig. S6H). The ATM/p53 target $p21^{CIP1}$ promotes cell cycle arrest, blocks apoptosis and can induce senescence on its own (Kagawa et al., 1999). When combined with the Aurora B or PLK1 inhibitors, $p21^{CIP1}$ overexpression rescued the binucleate cells from death (Castedo et al., 2004), yielding nearly homogeneous senescence (Fig. S6E and H, Movie S4).

Discussion

DNA-PKcs is a phosphatidylinositol 3-kinase-related kinase (PIKK) activated by binding of its Ku70 and Ku80 partners to DNA ends (Suwa et al., 1994). The search for endogenous substrates initially led to transcription factors such as p53, Sp1, c-Myc, and c-Jun but eventually yielded a wide range of other proteins (Goodwin and Knudsen, 2014). Mutant cells display DNA repair defects, a prolonged proliferative arrest and decreased survival after exposure to radiation or other genotoxic agents (Lees-Miller et al., 1995). While attention initially focused on p53 activation, DNA-PKcs was also found to phosphorylate the Ku proteins along with other NHEJ factors including XRCC4, Lig4 and XLF, implicating DNA-PKcs in non-homologous end joining (NHEJ), the primary mode of DSB repair throughout the cell cycle (Chang et al., 2017). Remarkably, our current understanding that DNA-PKcs serves an essential role in NHEJ repair appears to rely almost exclusively on studies in a small number of DNA-PKcs deficient cell lines (e.g. DNA-PKcs$^{-/-}$ MO59J human glioma (Lees-Miller et al., 1995)) and complementation with constructs derived from a reassembled DNA-PKcs cDNA (Kurimasa et al., 1999). A common feature of DNA-PKcs$^{-/-}$ models is the coinciding downregulation of ATM (Neal and Meek, 2019). Strikingly, Peng et al. (Peng et al., 2005) found that even a transient knockdown of DNA-PKcs with siRNA recapitulated this effect, resulting in loss of both ATM transcript and protein within days. Then, as the siRNA effects were lost, transcript and protein levels were restored not only for DNA-PKcs but also ATM. Perhaps, lacking negative regulation by DNA-PKcs (Finzel et al., 2016; Zhou et al., 2017), constitutively active ATM may induce autoregulatory factors (e.g. microRNA miR-100 (Ng et al., 2010; Zhang et al., 2011)) that mediate its downregulation. Thus, a caveat in assigning DNA-PKcs an essential role in DSB repair is that this ignores our long-standing knowledge of coregulation with ATM, which itself plays multiple roles in DNA damage response. In sum, while a direct role for DNA-PKcs in NHEJ is well accepted, it remains to be rigorously established. Nonetheless, only limited evidence has been published to date (e.g. (Sunada et al., 2016)) that appears to challenge the prevailing model.

Here, we showed that MCF7 human breast cancer cells either treated with the specific DNA-PKcs inhibitor Nu7026 and/or expressing an shRNA targeting DNA-PKcs displayed unperturbed DSB repair in neutral comet assays. By contrast, shRNA knockdown of Ku70, Ku80, Lig4 and other NHEJ factors (shNHEJ) conferred a dramatic repair defect after irradiation, whether DNA-PKcs was active or not. Arguing against alternative end joining compensating for the NHEJ defect (Iliakis, 2009), shRNA knockdowns of Lig3 and XRCC1 failed to block DNA-PKcs-independent DSB repair.

While we obtained no evidence for a role in NHEJ, DNA-PKcs activity was critical in mediating recovery from DNA damage response. Cells lacking DNA-PKcs displayed persistent γH2AX foci and cell proliferation arrest even after apparently completing DSB repair. In turn, despite a significant DSB repair defect in shNHEJ cells, γH2AX foci resolved on schedule and cells returned to proliferation. Moreover, inhibiting DNA-PKcs in shNHEJ cells led to γH2AX foci persistence and cell cycle arrest, confirming uncoupling between DNA damage and the DDR. Inhibiting ATM both blocked DSB repair and overcame the phenotypes of DNA-PKcs inhibition. A mechanism consistent with our data is for ATM to serve as the key driver that initiates and maintains the DDR and activates DSB repair while DNA-PKcs functions downstream, initially working in concert with ATM but then opposing ATM signaling to terminate the DDR. Remarkably, even when DSBs persist, the negative feedback from DNA-PKcs can still terminate the DDR. Indeed, inhibiting DNA-PKcs partly *suppressed* the DSB repair defect in shATM and several shNHEJ lines. Here, DNA-PKcs appears to antagonize DSB repair and promote aneuploidy rather than preserve genomic integrity.

Toward resolving the apparent paradox, our results are most consistent with recent studies establishing DNA-PKcs as a negative regulator of ATM after DNA damage (Zhou et al., 2017). A conservative model is that Ku70/80 heterodimer and ATM are recruited to DSBs, initiating the DNA damage response. Recruited by Ku, DNA-PKcs initially functions in concert with ATM to activate the DNA damage response. Together, they phosphorylate substrates in chromatin surrounding the DSB. Phosphorylation of H2AX at Ser139 in adjacent nucleosomes leads to γH2AX foci that promote DNA repair and induce cell cycle arrest (Fig. 6F). While ATM makes the major contribution to DDR activation, DNA-PKcs activity is critical for

normal recovery, mediated by downregulating ATM as DNA repair progresses. A model compatible with much of the literature is that Ku proteins bound at DSBs indeed recruit and activate DNA-PKcs kinase activity but also tether it in place. Our study suggests that subsequent release of active DNA-PKcs might serve as a mechanism to signal successful NHEJ repair, permitting downregulation of ATM and local foci resolution. Thus, in the absence of DNA-PKcs, while NHEJ can proceed, ATM remains active, resulting in γH2AX foci persistence, mitotic slippage and accelerated senescence. One inference is that the repair defects classically observed in DNA-PKcs deficient cell lines could reflect compensatory changes to accommodate ATM deregulation rather than loss of DNA-PKcs activity *per se*.

Nonetheless, our results do not rule out a specific role for DNA-PKcs in promoting DSB repair. One recent report found DNA-PKcs dispensable for rapid rejoining of compatible ends (Cary et al., 1997) but suggested a role in Lig4-mediated repair of complex damage (Reynolds et al., 2012). Complex DSBs may require end processing such as by the DNA-PKcs substrate Artemis, an endonuclease that accelerates NHEJ by clipping 5' overhangs (Ma et al., 2002). Nonetheless, the ^{60}Co gamma radiation (1.25 MeV) used here to induce DSBs produces more clustered damage than simple, ligatable breaks (Gulston et al., 2002), suggesting that DNA-PKcs-independent repair can also rejoin complex DSBs (Magnander and Elmroth, 2012). Further, despite lacking DNA-PKcs, yeast can perform rapid and efficient NHEJ of a wide range of lesions (Aylon and Kupiec, 2004), though other PIKKs may provide the critical functions. Even then, insofar as diverse prokaryotes (Weller et al., 2004) can perform end-joining repair and express homologs of Ku proteins and Lig4 (Weller et al., 2002) but appear to lack PIKKs altogether, DNA-PKcs was apparently not required for NHEJ for the first few billion years of evolution (Gu and Lieber, 2008).

Along with persistent γH2AX, we observed a profound cytokinesis defect, consistent with known roles for DNA-PKcs in cell division after DNA damage. Cells lacking DNA-PKcs performed mitosis and initiated cell division but displayed persistent cytoplasmic bridges that caused nascent daughter cells to collapse together, resulting in binucleate tetraploid cells that progressed to senescence. Consistent with prior work linking mitotic slippage to senescence (Panopoulos et al., 2014), we confirmed that inhibition of Aurora B or PLK1 was sufficient to produce cytokinetic failure and enhanced senescence in MCF7 cells, even without prior

irradiation. Taken together, the senescent phenotype after irradiation of cells lacking DNA-PKcs activity may be linked primarily to mitotic defects rather than any impacts on DNA repair.

The underlying rationale for development of DNA-PKcs inhibitors has long been to target NHEJ repair and thereby augment genotoxic cancer therapy. However, preclinical studies have begun to implicate alternative mechanisms of action. While Nu7441 induces chemo- and radio-sensitization in xenograft models (Ciszewski et al., 2014; Zhao et al., 2006), these effects may not depend on DSB repair (Sunada et al., 2016). The activity of the orally available DNA-PKcs inhibitor M3814 (nedisertib), an effective radiosensitizer in xenograft tumors (Damstrup et al., 2016) currently under investigation in clinical trials, has recently been ascribed to deregulation of ATM and p53 (Guo et al., 2018). Our data add to the emerging picture that the major role of DNA-PKcs in radiation tolerance may be in recovery after repair.

In conclusion, our study assigns DNA-PKcs a new primary role in the radiation response as the critical factor protecting cells against the deleterious effects of constitutive ATM activity. In the absence of DNA-PKcs, despite substantially completing DSB repair, unopposed ATM signaling leads to mitotic slippage and senescent arrest. Given concerns that therapy-induced senescence may be reversible (Chakradeo et al., 2016; Wang et al., 2013) and recent studies implicating inflammatory mediators released by senescent cells not only in tissue aging and carcinogenesis (Hoare and Narita, 2018) but also in driving adverse effects and resistance to therapy (Demaria et al., 2016), these findings suggest a reevaluation of DNA-PKcs as a cancer target.

Methods

Cell lines and cell culture

Human mammary carcinoma cell line MCF7$^{Tet\text{-}On}$ and Lenti-XTM293T cell line were obtained from Takara. Cell lines MDA-MB-435 (human melanoma), MDA-MB-231 (human breast cancer), B16-F10 (mouse melanoma), and CT26 (mouse colon cancer) were obtained from ATCC. The MCF7$^{GFP\text{-}IBD}$ cell line with GFP fused to the 53BP1 IRIF binding domain (IBD) under tetracycline-inducible control has been reported previously (Efimova et al., 2010). A previously described MCF7 cell line with FUCCI cell cycle reporter constructs (Sakaue-Sawano et al., 2008) was reconstructed here by transduction with lentivirus expressing mVenus-hGeminin (1/110)/pCSII-EF-MCS and mCherry-hCdt1 (30/120)/pCSII-EF-MCS. Cells with positive expression were selected by fluorescence-activated cell sorting (FACS).

Human cells were maintained in DMEM medium containing 4.5 g/L glucose (Thermo) supplemented with 10% Tet-approved FBS (Atlanta Biologicals) and 1% penicillin/streptomycin (Thermo). Mouse cells were maintained in RPMI 1640 medium (Thermo) supplemented with 10% Tet-approved FBS (Atlanta Biologicals) and 1% penicillin/streptomycin (Thermo). The cells were tested for mycoplasma and authenticated by short tandem repeat profile (IDEXX BioResearch) prior to performing experiments. All experiments were performed within 3 to 10 passages after thawing cells. Cells were treated with small molecules or DMSO vehicle 1 h before irradiation. All chemical probes used in this study are listed in Table S 1.

shRNA knockdowns

Pairs of Sigma MISSION shRNAs targeting expression of PRKDC (DNA-PKcs), ATM, RNF144A, XRCC6 (Ku70), XRCC5 (Ku80), Lig4, 53BP1, PAXX, XRCC4, XLF, Lig3, XRCC1, and a non-targeting scrambled (Scr) negative control were obtained as pLKO.1-puro vectors and used according to manufacturer's instructions. Lentivirus-containing supernatant was produced by transfection of the 293T Lenti-X cell line with corresponding plasmids and packaged plasmid mix and applied to MCF7$^{Tet\text{-}On}$ (Takara) cells. Following selection in the presence of puromycin, pairs of stable MCF7$^{Tet\text{-}On}$ cell lines with silencing of PRKDC, ATM, RNF144A, XRCC6, XRCC5, Lig4, 53BP1, PAXX, XRCC4, XLF, Lig3 and XRCC1

protein expression were established. Cells from the third passage post-selection were frozen in liquid N_2 as a stock and most experiments were performed within 4-10 passages. At least 2 shRNA constructs targeting different sequences of the corresponding mRNA were evaluated for each gene. Cells were collected from passage 2 or passage 3 after selection with puromycin and whole cell lysates were extracted. Silencing of targeted genes was validated by Western blot (Fig. S1A) and the shRNA with greatest apparent knock-down based on protein expression was used for experiments. Phenotypes were validated by shRNAs conferring consistent effects on formation and resolution of foci compared to scrambled control. shRNAs and antibodies used in this study are described in Supplemental Tables 2 and 3.

Clonogenic assays

Cells were plated at 100 cells per well in 6 well plates in triplicate and irradiated with doses of 1, 2, 3 and 4 Gy using a GammaCell ^{60}Co source (MDS Nordion) with dose rate ranging from 10.5 to 9.4 cGy/sec depending on the date of the experiment. Cells remained in culture for 3 weeks before staining with crystal violet (0.5%) and colonies of at least 50 cells were counted.

Neutral comet assays

For neutral comet assays, cells were seeded at 1 x 10^5 per well in 6-well plates prior to irradiation. After 24 h, cells were mixed with Comet LM agarose and single cell electrophoresis was performed on CometSlides (Trevigen). Slides were fixed, dried, stained with SYBR green (Thermo) and imaged on a Zeiss Axiovert 40CFL with a 10X Plan-NeoFluar objective and AxioCam digital camera controlled by AxioVision 4.8 software. Two or more replicates were performed. Images were analyzed using an ImageJ comet assay macro (http://www.med.unc.edu/microscopy/resources/imagejplugins-and-macros/comet-assay) and plugin OpenComet (Gyori et al., 2014) (http://www.cometbio.org/index.html).

Ionizing radiation-induced foci imaging

To image ionizing radiation-induced foci (IRIF), MCF7$^{GFP\text{-}IBD}$ cells were seeded on cover glass at 2.5 x 10^4 per well in 24 well plates. Expression of the GFP-IBD reporter was induced with 1 μg/mL doxycycline treatment for 48 h. After treatment with DNA-PKcs and/or ATM inhibitors, cells were fixed with 4% PFA at the indicated time point, stained with 5 μg/mL Hoechst 33342 (Sigma-Aldrich), and mounted using ProLong Gold (Invitrogen). For immunofluorescence staining, cells were fixed with 4% PFA and permeabilized with 10% Triton-X 100 for 10 min. After blocking with 5% BSA, primary antibodies for γH2AX (Millipore, 05-636, 1:1000) or 53BP1 (Novus, NB100-304, 1:1000) were then incubated on cell slides overnight at 4° C. Following PBS washes, fluorescent secondary antibodies (Jackson ImmunoResearch) were applied for 1 h at room temperature. Cell slides were mounted with ProLong Gold after PBS washes. Foci images were captured on an Zeiss Axiovert 40CFL with a 40X Plan-NeoFluar objective and pseudo-colored using ImageJ. Two or more replicates were performed.

SA-βGal assay

Cells were seeded at 3 x 10^4 per well in 6-well plates and treated with inhibitors for 1 h prior to irradiation. Cells were fixed after 4 or 5 days and assayed for SA-βGal activity as described (Efimova et al., 2010). Images were captured on a Zeiss Axiovert 200M microscope with 20X Plan-NeoFluar objective and Axiocam digital camera controlled by OpenLab software. SA-βGal positive and negative cells were counted in multiple fields, yielding an average percentage indicated on each SA-βGal image as mean ± SEM. Two or more replicates were performed.

Western blotting

5 x 10^5 cells were plated in P-100 Petri dishes and cells were harvested after 48 h. Whole cell lysates were prepared using M-PER lysis reagent (Thermo) in the presence of protease and phosphatase inhibitors (Thermo). 20 μg of protein was loaded per well, separated on a NuPage 3-8% Tris-Acetate precast gels (Invitrogen), and transferred onto PVDF membrane (EMB Millipore). After dividing blots into strips by apparent MW, immunoblotting was performed using primary antibodies including anti-DNA-PKcs, anti-phospho-DNA-PKcs, anti-γH2AX and anti-actin and detected

with peroxidase-conjugated secondary antibodies (Thermo, NA934vs or NA931). This was followed by detection with ECL peroxidase substrate (Thermo).

Flow cytometry

For sample preparation, MCF7 cells were collected 24 h after irradiation, then fixed with 2% PFA for 10 min on ice and permeabilized with 90% ice-cold methanol. Following blocking with 1% BSA, cells were incubated with an Alexa Flour 647 conjugated anti-γH2AX (anti-H2AX phosphoserine 139, Cell Signaling Technology, CST9720, 1:50) for 2 h and then washed using 1% BSA. 3 µg/ml DAPI was added to samples for DNA staining 15 min before flow cytometry. Flow cytometric data were acquired using a BD Fortessa X20 using FACSDiva software. 50,000 viable cells were acquired per sample. Flow cytometric data were analyzed using FlowJo software.

Time-lapse live cell analysis

ShScr, shDNA-PKcs or MCF7-FUCCI cells were seeded in a 6-well plate with 30,000 cells per well. After 24 h in culture, cells were treated with DMSO or Nu7026 and/or irradiated with 6 Gy. The plates were then analyzed by time-lapse in an IncuCyteS3 live cell imaging system. Phase contrast, green and red channel images were acquired at 20X magnification with scanning every 2 h for 7 d. More than 25 non-overlapping fields were captured for each well. Quantitative analysis of cell confluency was performed using IncuCyteS3 2018 software.

Fluorescence recovery after photobleaching (FRAP) analysis

Photobleaching was carried out on MCF7$^{GFP\text{-}IBD}$ cells after doxycycline induction. A 40X oil immersion objective of Leica SP8 laser scanning confocal microscope was used for all FRAP experiments. Photobleaching was achieved with 405 nm laser excitation for 10 s at full intensity. Data acquisition was performed with an excitation at 488 nm with 40% intensity for image scanning. At least 10 independent experiments were performed for each condition. Cells were imaged every second. ROI of the bleached area was acquired by ImageJ and normalized with easyFRAP (Rapsomaniki et al., 2012). Fluorescence recovery plots were fitted to a one-phase association exponential curve.

Statistical analysis

Statistical significance for anti-γH2AX, anti-53BP1 and GFP-IBD foci counting and comet assays was determined using the non-paired Student's t test. Calculations were performed using Prism software (GraphPad) or Excel. P values ≤ 0.05 were considered statistically significant.

Acknowledgements

We thank our colleagues for helpful support including Julian Lutze for comments on the manuscript and Liuyun Wu and Jordan Cooper for data analysis.

Competing interests

S.J.K. receives research grant funding to their laboratory from AbbVie for studies with PARP inhibitors and their spouse is a consultant for multiple pharmaceutical companies on cardiovascular genetics. S.J.K. has ownership interests in Cell IDx and Transnostics, private biotechnology companies focused on cancer diagnostics.

Funding

This work was funded by the NIH via R01s CA176843 and CA217182 to S.J.K.

Data availability

The primary data obtained for this study are available from the authors upon reasonable request. Source data for Fig. 1D are available with the paper online.

References

Aylon, Y. and Kupiec, M. (2004). DSB repair: the yeast paradigm. *DNA repair* **3**, 797-815.

Azad, A., Jackson, S., Cullinane, C., Natoli, A., Neilsen, P. M., Callen, D. F., Maira, S.-M., Hackl, W., McArthur, G. A. and Solomon, B. (2011). Inhibition of DNA-Dependent Protein Kinase Induces Accelerated Senescence in Irradiated Human Cancer Cells. *Molecular Cancer Research* **9**, 1696-1707.

Blackford, A. N. and Jackson, S. P. (2017). ATM, ATR, and DNA-PK: the trinity at the heart of the DNA damage response. *Molecular cell* **66**, 801-817.

Bouquet, F., Muller, C. and Salles, B. (2006). The loss of γH2AX signal is a marker of DNA double strand breaks repair only at low levels of DNA damage. *Cell cycle* **5**, 1116-1122.

Burma, S., Chen, B. P., Murphy, M., Kurimasa, A. and Chen, D. J. (2001). ATM phosphorylates histone H2AX in response to DNA double-strand breaks. *Journal of Biological Chemistry* **276**, 42462-42467.

Cary, R. B., Peterson, S. R., Wang, J., Bear, D. G., Bradbury, E. M. and Chen, D. J. (1997). DNA looping by Ku and the DNA-dependent protein kinase. *Proceedings of the National Academy of Sciences* **94**, 4267-4272.

Castedo, M., Perfettini, J.-L., Roumier, T., Andreau, K., Medema, R. and Kroemer, G. (2004). Cell death by mitotic catastrophe: a molecular definition. *Oncogene* **23**, 2825.

Chakradeo, S., W Elmore, L. and A Gewirtz, D. (2016). Is senescence reversible? *Current drug targets* **17**, 460-466.

Chang, H. H., Pannunzio, N. R., Adachi, N. and Lieber, M. R. (2017). Non-homologous DNA end joining and alternative pathways to double-strand break repair. *Nature reviews Molecular cell biology* **18**, 495.

Chen, B. P., Uematsu, N., Kobayashi, J., Lerenthal, Y., Krempler, A., Yajima, H., Löbrich, M., Shiloh, Y. and Chen, D. J. (2007). Ataxia telangiectasia mutated (ATM) is essential for DNA-PKcs phosphorylations at the Thr-2609 cluster upon DNA double strand break. *Journal of Biological Chemistry* **282**, 6582-6587.

Ciccia, A. and Elledge, S. J. (2010). The DNA damage response: making it safe to play with knives. *Molecular cell* **40**, 179-204.

Ciszewski, W. M., Tavecchio, M., Dastych, J. and Curtin, N. J. (2014). DNA-PK inhibition by NU7441 sensitizes breast cancer cells to ionizing radiation and doxorubicin. *Breast cancer research and treatment* **143**, 47-55.

Damstrup, L., Zimmerman, A., Sirrenberg, C., Zenke, F. and Vassilev, L. (2016). M3814, a DNA-dependent protein Kinase inhibitor (DNA-PKi), potentiates the effect of ionizing radiation (IR) in Xenotransplanted Tumors in nude mice. *International Journal of Radiation Oncology• Biology• Physics* **94**, 940-941.

Davidson, D., Amrein, L., Panasci, L. and Aloyz, R. (2013). Small molecules, inhibitors of DNA-PK, targeting DNA repair, and beyond. *Frontiers in pharmacology* **4**, 5.

De Santis Puzzonia, M., Gonzalez, L., Ascenzi, S., Cundari, E. and Degrassi, F. (2016). Tetraploid cells produced by absence of substrate adhesion during cytokinesis are limited in their proliferation and enter senescence after DNA replication. *Cell cycle* **15**, 274-282.

Demaria, M., O'Leary, M. N., Chang, J., Shao, L., Liu, S., Alimirah, F., Koenig, K., Le, C., Mitin, N. and Deal, A. M. (2016). Cellular senescence promotes adverse effects of chemotherapy and cancer relapse. *Cancer discovery*, 165-176.

Douglas, P., Ye, R., Trinkle-Mulcahy, L., Neal, J. A., De Wever, V., Morrice, N. A., Meek, K. and Lees-Miller, S. P. (2014). Polo-like kinase 1 (PLK1) and protein phosphatase 6 (PP6) regulate DNA-dependent protein kinase catalytic subunit (DNA-PKcs) phosphorylation in mitosis. *Bioscience reports* **34**, e00113.

Efimova, E. V., Mauceri, H. J., Golden, D. W., Labay, E., Bindokas, V. P., Darga, T. E., Chakraborty, C., Barreto-Andrade, J. C., Crawley, C. and Sutton, H. G. (2010). Poly (ADP-ribose) polymerase inhibitor induces accelerated senescence in irradiated breast cancer cells and tumors. *Cancer research*, 0008-5472. CAN-09-4224.

Fededa, J. P. and Gerlich, D. W. (2012). Molecular control of animal cell cytokinesis. *Nature cell biology* **14**, 440.

Finzel, A., Grybowski, A., Strasen, J., Cristiano, E. and Loewer, A. (2016). Hyperactivation of ATM upon DNA-PKcs inhibition modulates p53 dynamics and cell fate in response to DNA damage. *Molecular biology of the cell* **27**, 2360-2367.

Fumagalli, M., Rossiello, F., Mondello, C. and di Fagagna, F. d. A. (2014). Stable cellular senescence is associated with persistent DDR activation. *PloS one* **9**, e110969.

Goodwin, J. F. and Knudsen, K. E. (2014). Beyond DNA repair: DNA-PK function in cancer. *Cancer discovery* **4**, 1126-1139.

Gu, J. and Lieber, M. R. (2008). Mechanistic flexibility as a conserved theme across 3 billion years of nonhomologous DNA end-joining. *Genes & development* **22**, 411-415.

Gulston, M., Fulford, J., Jenner, T., de Lara, C. and O'neill, P. (2002). Clustered DNA damage induced by γ radiation in human fibroblasts (HF19), hamster (V79-4) cells and plasmid DNA is revealed as Fpg and Nth sensitive sites. *Nucleic acids research* **30**, 3464-3472.

Guo, Y., Sun, Q., Liu, X., Puc, J., Czauderna, F., Zenke, F., Blaukat, A. and Vassilev, L. T. (2018). Pharmacological DNA-PK inhibition induces ATM/p53 dependent premature senescence with immunomodulatory phenotype in irradiated cancer cells. *AACR Annual Meeting*, 982.

Gyori, B. M., Venkatachalam, G., Thiagarajan, P., Hsu, D. and Clement, M.-V. (2014). OpenComet: an automated tool for comet assay image analysis. *Redox biology* **2**, 457-465.

Hartlerode, A. J., Morgan, M. J., Wu, Y., Buis, J. and Ferguson, D. O. (2015). Recruitment and activation of the ATM kinase in the absence of DNA-damage sensors. *Nature Structural and Molecular Biology* **22**, 736.

Hickson, I., Zhao, Y., Richardson, C. J., Green, S. J., Martin, N. M., Orr, A. I., Reaper, P. M., Jackson, S. P., Curtin, N. J. and Smith, G. C. (2004). Identification and characterization of a novel and specific inhibitor of the ataxia-telangiectasia mutated kinase ATM. *Cancer research* **64**, 9152-9159.

Ho, S.-R., Mahanic, C. S., Lee, Y.-J. and Lin, W.-C. (2014). RNF144A, an E3 ubiquitin ligase for DNA-PKcs, promotes apoptosis during DNA damage. *Proceedings of the National Academy of Sciences* **111**, E2646-E2655.

Hoare, M. and Narita, M. (2018). The Power Behind the Throne: Senescence and the Hallmarks of Cancer. *Annual Review of Cancer Biology* **2**, 175-194.

Iliakis, G. (2009). Backup pathways of NHEJ in cells of higher eukaryotes: cell cycle dependence. *Radiotherapy and Oncology* **92**, 310-315.

Jette, N. and Lees-Miller, S. P. (2015). The DNA-dependent protein kinase: A multifunctional protein kinase with roles in DNA double strand break repair and mitosis. *Progress in biophysics and molecular biology* **117**, 194-205.

Kagawa, S., Fujiwara, T., Kadowaki, Y., Fukazawa, T., Sok-Joo, R., Roth, J. A. and Tanaka, N. (1999). Overexpression of the p21 p21 sdi1 gene induces senescence-like state in human cancer cells: implication for senescence-directed molecular therapy for cancer. *Cell death and differentiation* **6**, 765.

Kang, H. T., Park, J. T., Choi, K., Kim, Y., Choi, H. J. C., Jung, C. W., Lee, Y.-S. and Park, S. C. (2017). Chemical screening identifies ATM as a target for alleviating senescence. *Nature chemical biology* **13**, 616.

Kurimasa, A., Kumano, S., Boubnov, N. V., Story, M. D., Tung, C.-S., Peterson, S. R. and Chen, D. J. (1999). Requirement for the kinase activity of human DNA-dependent protein kinase catalytic subunit in DNA strand break rejoining. *Molecular and cellular biology* **19**, 3877-3884.

Leahy, J. J., Golding, B. T., Griffin, R. J., Hardcastle, I. R., Richardson, C., Rigoreau, L. and Smith, G. C. (2004). Identification of a highly potent and selective DNA-dependent protein kinase (DNA-PK) inhibitor (NU7441) by screening of chromenone libraries. *Bioorganic & medicinal chemistry letters* **14**, 6083-6087.

Lees-Miller, S. P., Godbout, R., Chan, D. W., Weinfeld, M., Day, R. S., Barron, G. M. and Allalunis-Turner, J. (1995). Absence of p350 subunit of DNA-activated protein kinase from a radiosensitive human cell line. *Science* **267**, 1183-1185.

Lieber, M. R. (2010). NHEJ and its backup pathways in chromosomal translocations. *Nature Structural and Molecular Biology* **17**, 393.

Ma, Y., Pannicke, U., Schwarz, K. and Lieber, M. R. (2002). Hairpin opening and overhang processing by an Artemis/DNA-dependent protein kinase complex in nonhomologous end joining and V (D) J recombination. *Cell* **108**, 781-794.

Magnander, K. and Elmroth, K. (2012). Biological consequences of formation and repair of complex DNA damage. *Cancer letters* **327**, 90-96.

Neal, J. A. and Meek, K. (2019). Deciphering phenotypic variance in different models of DNA-PKcs deficiency. *DNA repair* **73**, 7-16.

Ng, W. L., Yan, D., Zhang, X., Mo, Y.-Y. and Wang, Y. (2010). Over-expression of miR-100 is responsible for the low-expression of ATM in the human glioma cell line: M059J. *DNA repair* **9**, 1170-1175.

Nutley, B., Smith, N., Hayes, A., Kelland, L., Brunton, L., Golding, B., Smith, G., Martin, N., Workman, P. and Raynaud, F. (2005). Preclinical

pharmacokinetics and metabolism of a novel prototype DNA-PK inhibitor NU7026. *British journal of cancer* **93**, 1011.

O'Connor, M. J. (2015). Targeting the DNA damage response in cancer. *Molecular cell* **60**, 547-560.

Panier, S. and Boulton, S. J. (2014). Double-strand break repair: 53BP1 comes into focus. *Nature reviews Molecular cell biology* **15**, 7.

Panopoulos, A., Pacios-Bras, C., Choi, J., Yenjerla, M., Sussman, M. A., Fotedar, R. and Margolis, R. L. (2014). Failure of cell cleavage induces senescence in tetraploid primary cells. *Molecular biology of the cell* **25**, 3105-3118.

Pearl, L. H., Schierz, A. C., Ward, S. E., Al-Lazikani, B. and Pearl, F. M. (2015). Therapeutic opportunities within the DNA damage response. *Nature Reviews Cancer* **15**, 166.

Peng, Y., Woods, R. G., Beamish, H., Ye, R., Lees-Miller, S. P., Lavin, M. F. and Bedford, J. S. (2005). Deficiency in the catalytic subunit of DNA-dependent protein kinase causes down-regulation of ATM. *Cancer research* **65**, 1670-1677.

Rapsomaniki, M. A., Kotsantis, P., Symeonidou, I.-E., Giakoumakis, N.-N., Taraviras, S. and Lygerou, Z. (2012). easyFRAP: an interactive, easy-to-use tool for qualitative and quantitative analysis of FRAP data. *Bioinformatics* **28**, 1800-1801.

Reynolds, P., Anderson, J. A., Harper, J. V., Hill, M. A., Botchway, S. W., Parker, A. W. and O'neill, P. (2012). The dynamics of Ku70/80 and DNA-PKcs at DSBs induced by ionizing radiation is dependent on the complexity of damage. *Nucleic acids research* **40**, 10821-10831.

Rodier, F., Coppé, J.-P., Patil, C. K., Hoeijmakers, W. A., Muñoz, D. P., Raza, S. R., Freund, A., Campeau, E., Davalos, A. R. and Campisi, J. (2009). Persistent DNA damage signalling triggers senescence-associated inflammatory cytokine secretion. *Nature cell biology* **11**, 973.

Rogakou, E. P., Pilch, D. R., Orr, A. H., Ivanova, V. S. and Bonner, W. M. (1998). DNA double-stranded breaks induce histone H2AX phosphorylation on serine 139. *Journal of Biological Chemistry* **273**, 5858-5868.

Sakaue-Sawano, A., Kurokawa, H., Morimura, T., Hanyu, A., Hama, H., Osawa, H., Kashiwagi, S., Fukami, K., Miyata, T. and Miyoshi, H. (2008). Visualizing spatiotemporal dynamics of multicellular cell-cycle progression. *Cell* **132**, 487-498.

Salles, B., Calsou, P., Frit, P. and Muller, C. (2006). The DNA repair complex DNA-PK, a pharmacological target in cancer chemotherapy and radiotherapy. *Pathologie Biologie* **54**, 185-193.

Schultz, L. B., Chehab, N. H., Malikzay, A. and Halazonetis, T. D. (2000). p53 binding protein 1 (53BP1) is an early participant in the cellular response to DNA double-strand breaks. *The Journal of cell biology* **151**, 1381-1390.

Shang, Z.-F., Huang, B., Xu, Q.-Z., Zhang, S.-M., Fan, R., Liu, X.-D., Wang, Y. and Zhou, P.-K. (2010). Inactivation of DNA-dependent protein kinase leads to spindle disruption and mitotic catastrophe with attenuated checkpoint protein 2 Phosphorylation in response to DNA damage. *Cancer research* **70**, 3657-3666.

Stiff, T., O'Driscoll, M., Rief, N., Iwabuchi, K., Löbrich, M. and Jeggo, P. A. (2004). ATM and DNA-PK function redundantly to phosphorylate H2AX after exposure to ionizing radiation. *Cancer research* **64**, 2390-2396.

Sunada, S., Kanai, H., Lee, Y., Yasuda, T., Hirakawa, H., Liu, C., Fujimori, A., Uesaka, M. and Okayasu, R. (2016). Nontoxic concentration of DNA-PK inhibitor NU7441 radio-sensitizes lung tumor cells with little effect on double strand break repair. *Cancer science* **107**, 1250-1255.

Suwa, A., Hirakata, M., Takeda, Y., Jesch, S. A., Mimori, T. and Hardin, J. A. (1994). DNA-dependent protein kinase (Ku protein-p350 complex) assembles on double-stranded DNA. *Proceedings of the National Academy of Sciences* **91**, 6904-6908.

Wang, Q., Wu, P. C., Dong, D. Z., Ivanova, I., Chu, E., Zeliadt, S., Vesselle, H. and Wu, D. Y. (2013). Polyploidy road to therapy-induced cellular senescence and escape. *International journal of cancer* **132**, 1505-1515.

Weller, G. R., Brandt, V. L. and Roth, D. B. (2004). Doing more with less in bacterial DNA repair. *Nature Structural and Molecular Biology* **11**, 1158.

Weller, G. R., Kysela, B., Roy, R., Tonkin, L. M., Scanlan, E., Della, M., Devine, S. K., Day, J. P., Wilkinson, A. and di Fagagna, F. d. A. (2002). Identification of a DNA nonhomologous end-joining complex in bacteria. *Science* **297**, 1686-1689.

Yang, J., Yu, Y., Hamrick, H. E. and Duerksen-Hughes, P. J. (2003). ATM, ATR and DNA-PK: initiators of the cellular genotoxic stress responses. *Carcinogenesis* **24**, 1571-1580.

You, Z., Bailis, J. M., Johnson, S. A., Dilworth, S. M. and Hunter, T. (2007). Rapid activation of ATM on DNA flanking double-strand breaks. *Nature cell biology* **9**, 1311.

Zhang, X., Wan, G., Berger, F. G., He, X. and Lu, X. (2011). The ATM kinase induces microRNA biogenesis in the DNA damage response. *Molecular cell* **41**, 371-383.

Zhao, Y., Thomas, H. D., Batey, M. A., Cowell, I. G., Richardson, C. J., Griffin, R. J., Calvert, A. H., Newell, D. R., Smith, G. C. and Curtin, N. J. (2006). Preclinical evaluation of a potent novel DNA-dependent protein kinase inhibitor NU7441. *Cancer research* **66**, 5354-5362.

Zhou, Y., Lee, J.-H., Jiang, W., Crowe, J. L., Zha, S. and Paull, T. T. (2017). Regulation of the DNA damage response by DNA-PKcs inhibitory phosphorylation of ATM. *Molecular cell* **65**, 91-104.

Figures

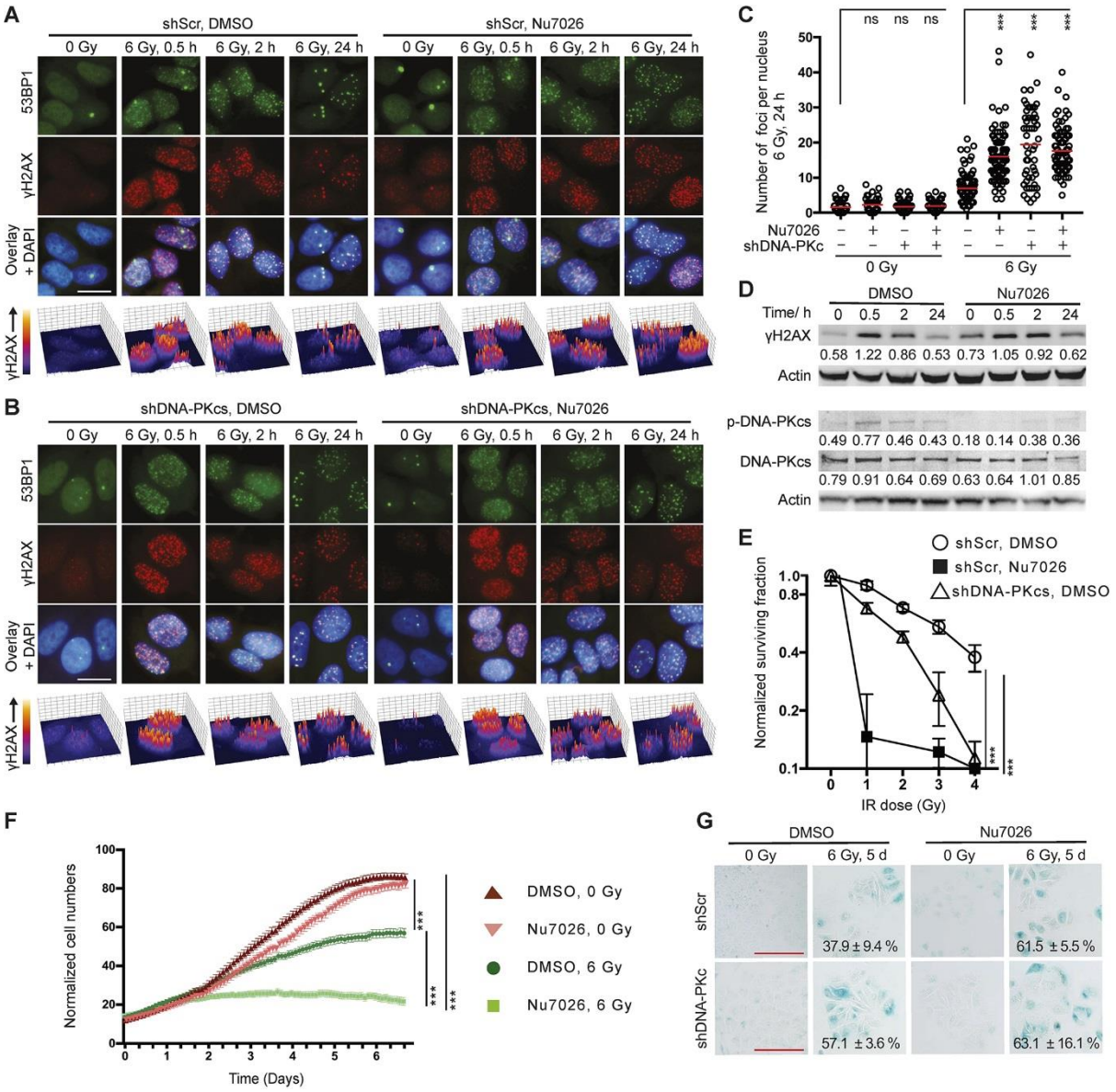

Fig. 1: Inhibition of DNA-PKcs induces persistent γH2AX foci, enhanced radiosensitivity and accelerated cellular senescence

A, B. Immunofluorescence staining of γH2AX and 53BP1 foci in MCF7 cells after irradiation. shScr control (**A**) and shDNA-PKcs (**B**) cells were treated with DMSO or DNA-PKcs inhibitor Nu7026 (10 μM) 1 h before 6 Gy ionizing radiation (IR) and cells were fixed at indicated times after IR. Shown are false-colored images of anti-53BP1 (green), anti-γH2AX (red), three color overlay with DAPI (blue), and perspective plots

of γH2AX staining intensity for representative examples from each condition. Images were colored and analyzed by ImageJ. Scale bar = 20 μm. **C.** Quantitation of γH2AX foci per nucleus in shScr or shDNA-PKcs treated with DMSO or Nu7026 at 24 h after 0 or 6 Gy IR. Data obtained from >100 cells (open circles) are shown as mean ± s.d. (red bar). **D.** Western analysis of time course of DNA damage response in shScr cells treated with 6 Gy in the presence of DMSO or Nu7026. Upper strips: γH2AX (phospho-Ser139) levels and ß-actin loading control. Lower strips: p-DNA-PKcs (phospho-Thr2609), total DNA-PKcs, and actin control. Normalized intensity indicated below each γH2AX and DNA-PKcs band. **E.** Clonogenic radiosensitivity assay comparing shScr treated with DMSO or Nu7026 (3 μM) and shDNA-PKcs. N=3, mean ± s.d. **F.** Automated proliferation analysis from time-lapse imaging over 7 d comparing shScr cells treated with DMSO or Nu7026 (3 μM) and then 0 or 6 Gy at time 0. **G.** Senescence-associated beta-galactosidase (SA-βGal) staining of shScr or shDNA-PKcs cells treated with DMSO or Nu7026 (3 μM) before 0 or 6 Gy and fixed after 5 d. Mean percentage ± s.d. of SA-βGal^{+} cells from five 20X fields indicated. Scale bar = 200 μm. For statistical analysis, data compared to shScr DMSO control by unpaired t-test, ***, $p < 0.001$; ns, $p > 0.05$.

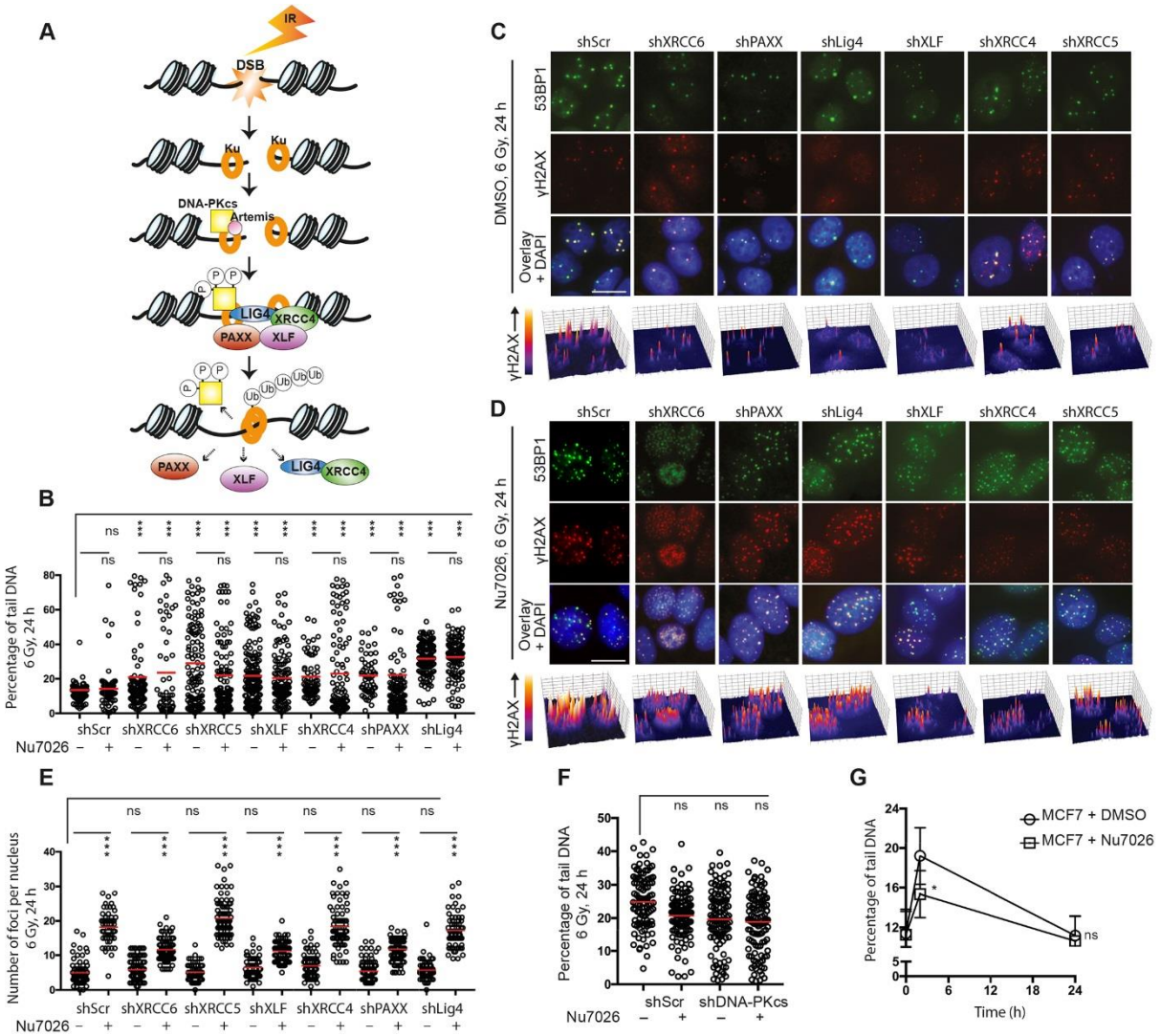

Fig. 2: Unrepaired DSBs are not sufficient to maintain persistent γH2AX foci

A. Schematic representation of current model for DSB repair by conventional non-homologous end joining (NHEJ). Upon DSB formation, the Ku70/80 heterodimer binds and recruits DNA-PKcs and Artemis, leading to assembly of factors which perform NHEJ and then disperse. Phosphorylated DNA-PKcs is released and Ku is degraded by Ub-mediated proteolysis, leaving behind a religated chromosome. **B.** Quantitative analysis of DSBs in shScr and shNHEJ lines. Cells were treated with DMSO or Nu7206 (10 μM) 1 h before 6 Gy, collected after 24 h and examined by neutral comet assay (single cell electrophoresis). Percent tail DNA was determined using OpenComet. **C. D.** Immunofluorescence analysis of γH2AX (red) and 53BP1 (green). shScr and shNHEJ were treated with DMSO (**C**) or Nu7026 (10 μM, **D**) 1 h before IR and stained 24 h after IR with anti-53BP1 (green) or anti-γH2AX (red).

Three color overlay with DAPI (blue) and perspective plots of γH2AX shown for representative examples. Scale bar = 20 μm. **E.** Quantitation of γH2AX foci per nucleus at 24 h after IR for samples in **C** and **D**. **F.** Quantitative analysis of DSBs in shScr and shDNA-PKcs cells treated and analyzed as in **B**. **G.** Time course comet assay results in shScr cells treated as in **B** and collected before IR (0 h), and at 2 h and 24 h after 6 Gy. In each case, data obtained from >100 cells (open circles) are shown as mean ± s.d. (red bar). Unpaired t-tests were performed, ***, $p < 0.001$; *, $p < 0.05$; ns, $p > 0.05$.

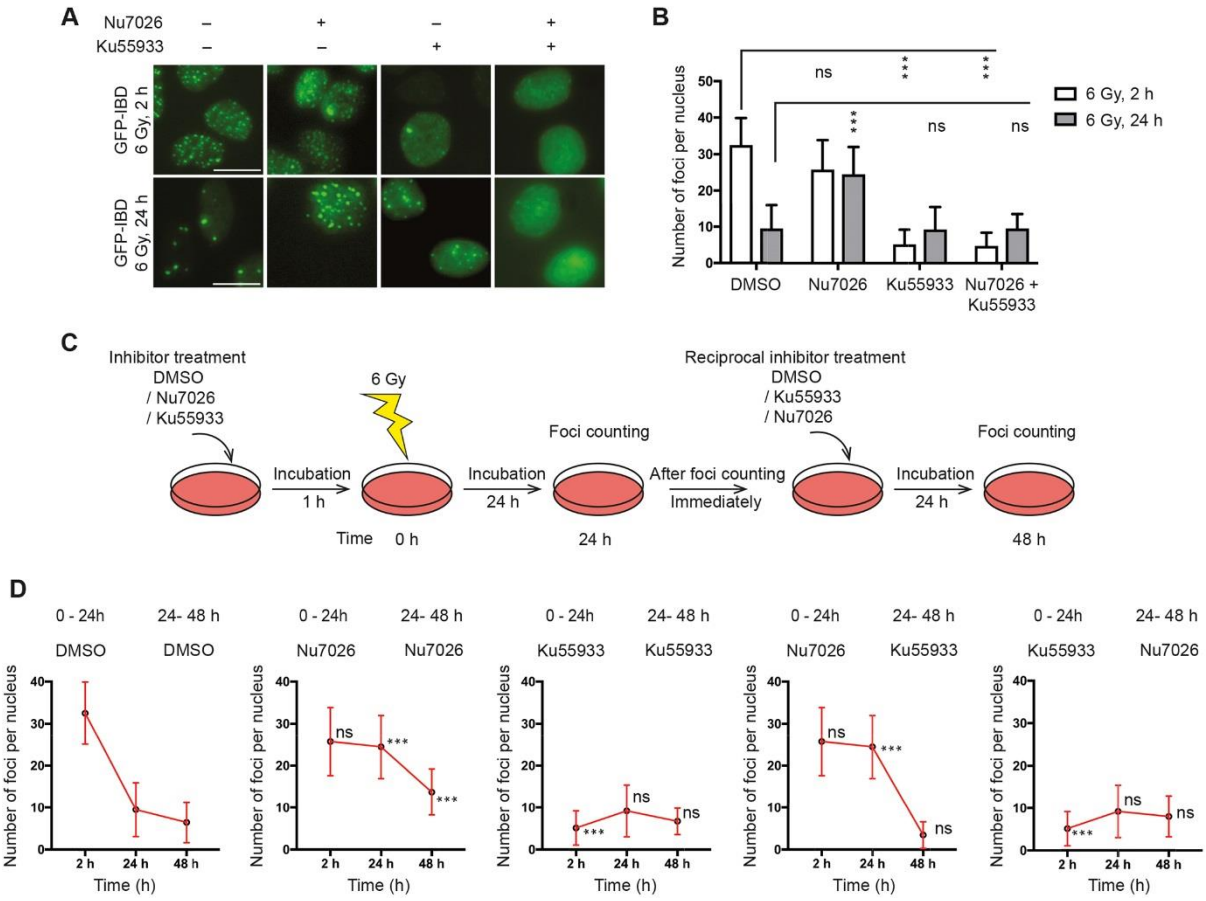

Fig. 3: ATM activity is required for both the initiation and maintenance of γH2AX foci.

A. Live-cell fluorescence imaging of GFP-IBD reporter for 53BP1 in MCF7 cells. MCF7$^{GFP\text{-}IBD}$ cells were treated with DNA-PKcs inhibitor Nu7026 (10 μM), ATM inhibitor Ku55933 (1 μM), or both 1 h before irradiation and images captured 2 h and 24 h after 6 Gy. Representative images are shown. Scale bar = 20 μm. **B.** Quantification of GFP-IBD foci as in **A** at 2 h and 24 h. **C.** Schematic of the sequential incubation experiment. shScr cells were treated with either Ku55933 or Nu7026 1 h before 6 Gy and imaged 24 h after irradiation. Then, reciprocal inhibitors were added for another 24 h incubation period. **D.** Quantification of GFP-IBD foci per nucleus in the sequential incubation experiment. N > 50 cells, mean± s.d. Unpaired t-tests at each time point compared to DMSO controls, ***, $p < 0.001$.

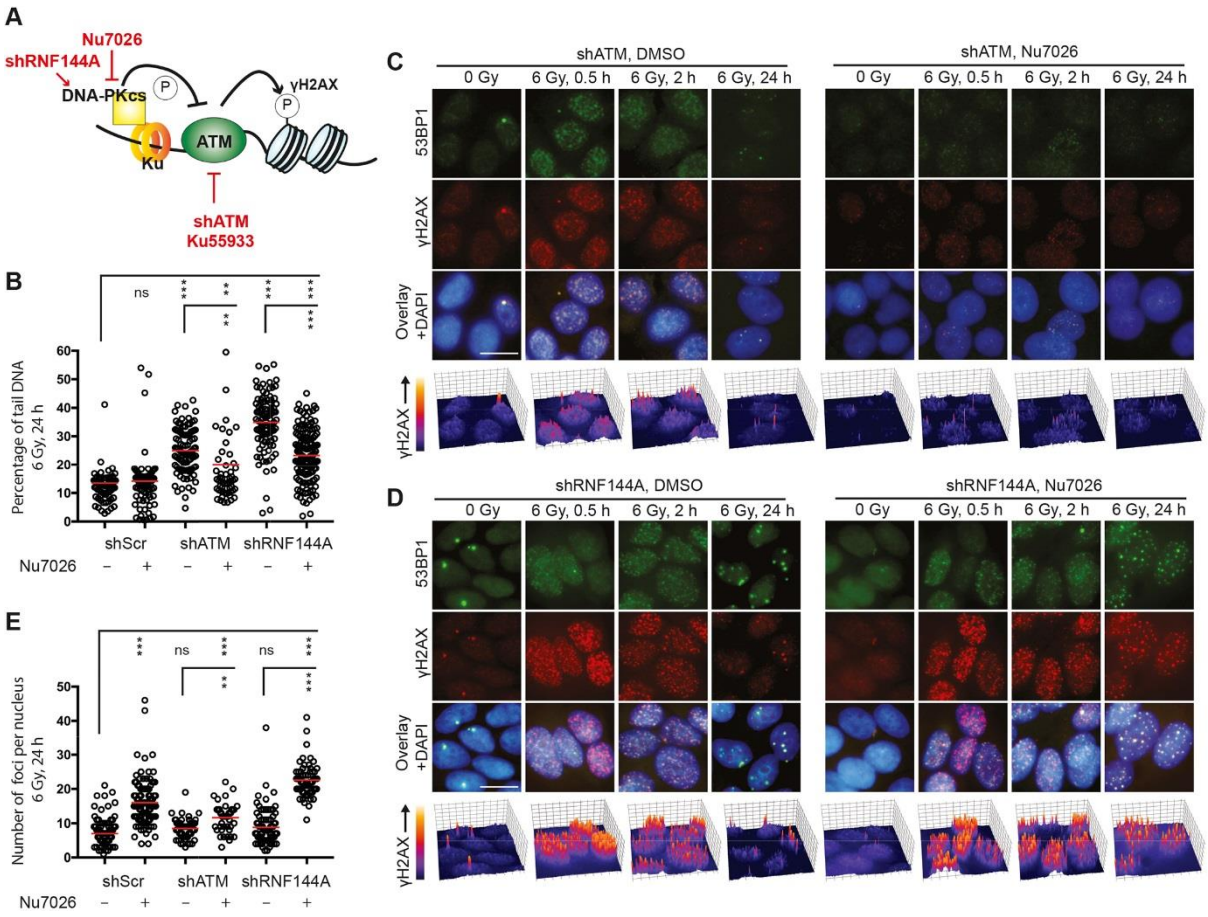

Fig. 4: DNA-PKcs regulates γH2AX foci resolution by attenuating ATM activity

A. Schematic representation of the interaction between DNA-PKcs and ATM at DSBs. In DNA damage response, ATM dominantly regulates H2AX phosphorylation and thus yields γH2AX; while DNA-PKcs mediated phosphorylation of ATM impairs ATM activity. ATM can be inhibited by shATM or Ku55933 and DNA-PKcs by Nu7026. shRNF-144A prevents degradation of DNA-PKcs. **B.** Quantitative analysis of DSBs in shScr, shATM, and shRNF-144A lines by neutral comet assay after treatment with DMSO or Nu7026 1 h before IR. Cells were collected 24 h after 6 Gy. **C. D**. Immunofluorescence analysis of γH2AX and 53BP1 in shATM (**C**) and shRNF-144A (**D**) treated with DMSO or Nu7026 (10 μM)1 h before IR and fixed at the indicated time points. Cells were stained 24 h after IR with anti-53BP1 (green) or anti-γH2AX (red). Three color overlay with DAPI (blue) and perspective plots of γH2AX shown for representative examples. Scale bar = 20 μm. **E.** Quantitation of γH2AX foci per nucleus at 24 h after IR for samples in **C** and **D**. Data obtained from >100 cells (open circles) are shown as mean ± s.d. (red bar). Unpaired t-tests were performed, ***, $p < 0.001$.

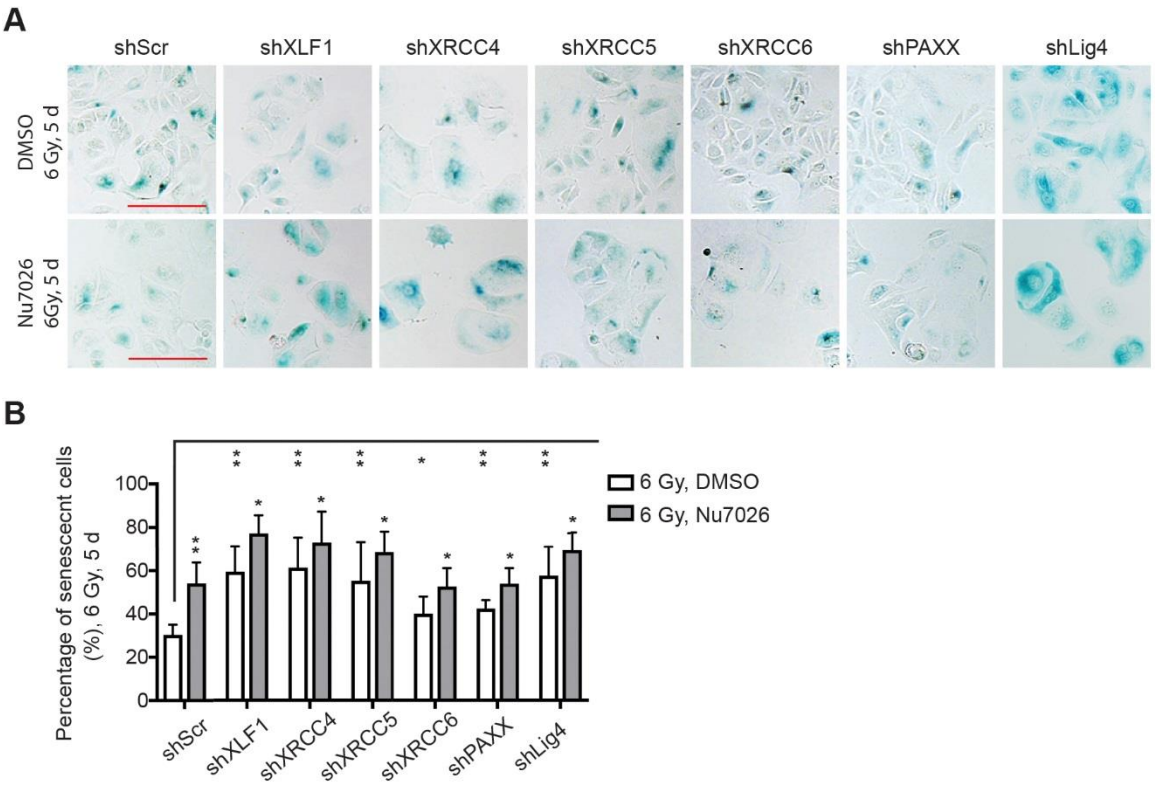

Fig. 5: DNA-PKcs inhibition augments cellular senescence in cells with NHEJ defects

A. Detection of accelerated senescence by SA-βGal staining. shScr and shNHEJ cell lines were treated with DMSO or Nu7026 (3 μM) 1 h before 6 Gy irradiation, incubated for 5 d and then fixed and stained. Representative images are displayed. Scale bar = 200 μm. **B.** Mean percentage of SA-βGal$^+$ ± s.d. for each condition determined from five 20X fields. Unpaired t-test, *, $p < 0.05$; **, $p<0.01$.

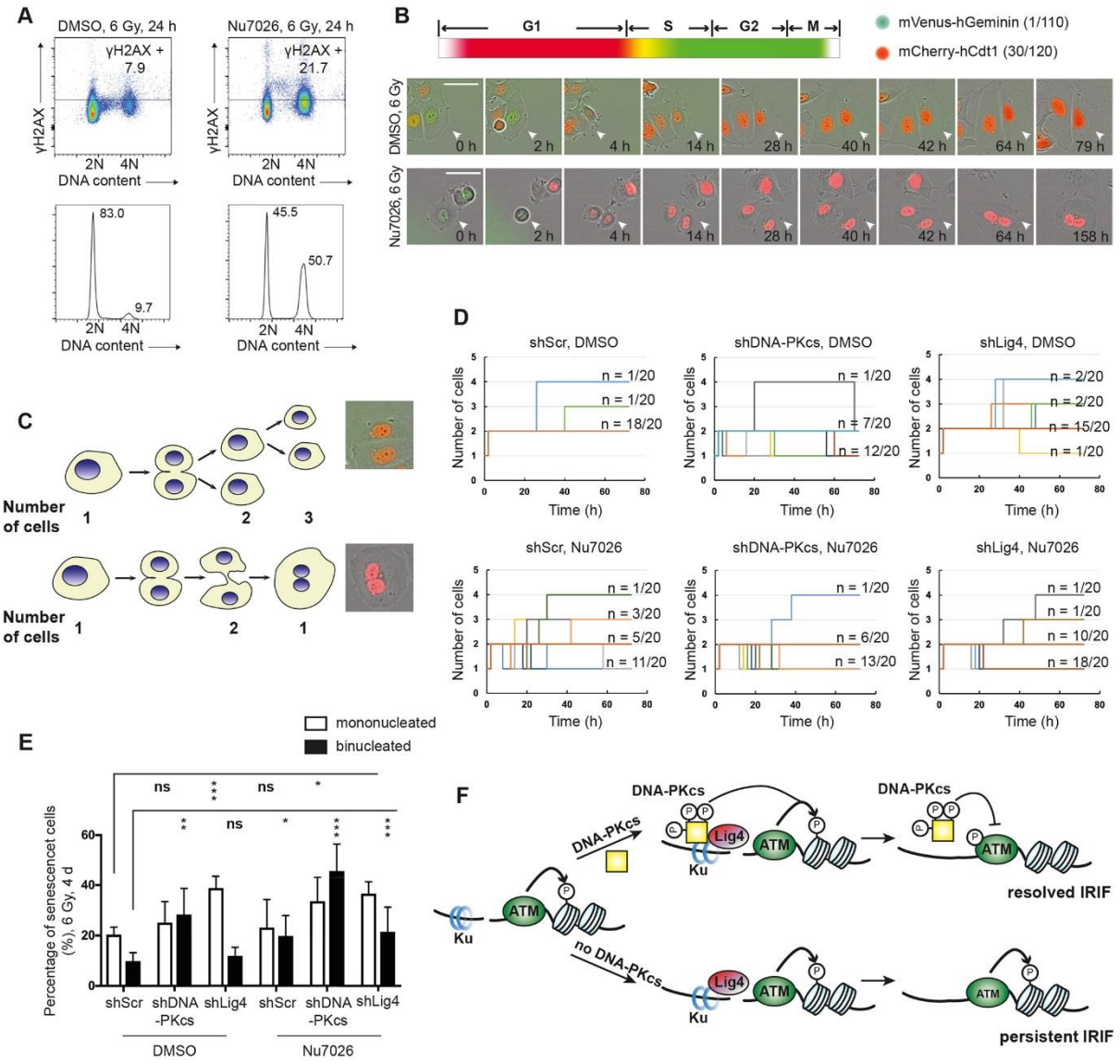

Fig. 6: Inhibition of DNA-PKcs causes cytokinesis defects and prolonged cell cycle arrest

A. Flow cytometry analysis of DNA content (DAPI) and γH2AX in cells treated with DMSO or Nu7026 (10 μM) 1 h before 6 Gy and then collected after 24 h. The 2D dot plots (upper) show γH2AX staining across the cell cycle. Total % γH2AX$^+$ was gated based on unirradiated cell sample. The histograms (lower) show relative abundance at each DNA content. Data acquired from 50,000 cells per sample. **B.** Time-lapse analysis of MCF7-FUCCI cells treated the same as in **A**. (Upper) Diagram represents fluorescent FUCCI reporter expression through the cell cycle. (Lower) Representative cells shown at indicated times. Carets indicate cells that perform mitosis and cytokinesis during time course. Scale bar = 50 μm. **C.** Schematic

diagrams of normal mitosis and mitotic slippage after irradiation. In normal mitosis (upper), the mother cell divides completely into two daughter cells. Each daughter can perform another cell division or become senescent. In mitotic slippage (lower), persistent cytoplasmic bridges between daughter cells precede collapse to reform a single cell that contains two nuclei, leading to cell death or senescence. **D.** Tracking cell division of single cells after irradiation. shScr, shDNA-PKcs and shLig4 cells were treated with DMSO or Nu7026 (3 μM) 1 h before 6 Gy. The time after IR at which rounding up for mitosis was first observed was set as 0 h. Then, 20 cells were tracked for each condition, revealing distinct trajectories of completed cell division and/or mitotic slippage. **E.** Analysis of senescent morphology in shScr, shDNA-PKcs and shLig4 cells treated as in **D** and tracked until 4 d after irradiation. Cells with senescent morphology were classified as mono- or bi-nucleated. Histogram shows mean ± s.d. N > 50. Unpaired t-test, *, $p < 0.05$; **, $p<0.01$. **F.** Schematic representation of the proposed functions of DNA-PKcs at DSBs. Initially, the Ku70/80 heterodimer and ATM are recruited to DSBs, initiating the DNA damage response, which includes phosphorylation of H2AX at Ser139 in adjacent nucleosomes leading to γH2AX foci. DNA-PKcs is recruited by Ku and activated by ATM. Thereby, in concert with ATM, DNA-PKcs can promote γH2AX foci formation and activation of the DNA damage response to induce checkpoint arrest. Once NHEJ completes DSB repair, active DNA-PK is released to down-regulate ATM, allowing γH2AX foci resolution and terminating the DNA damage response to promote cell division. Absence of DNA-PKcs does not prevent NHEJ but allows ATM to remain active, causing γH2AX foci persistence, mitotic slippage and accelerated senescence.

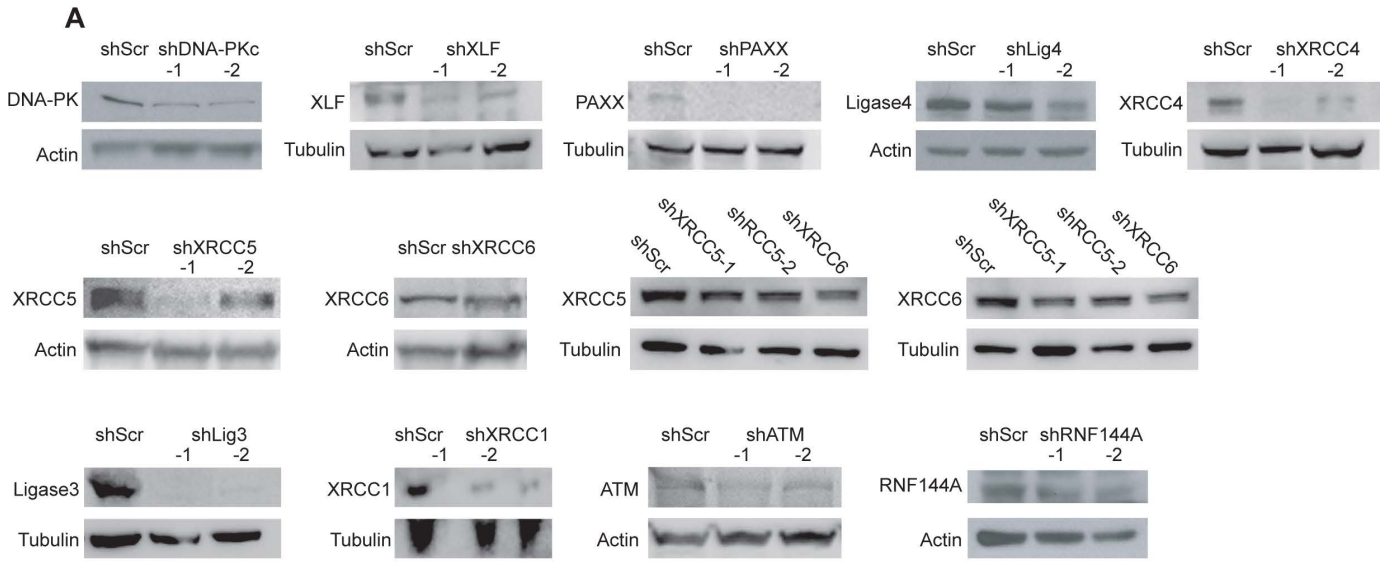

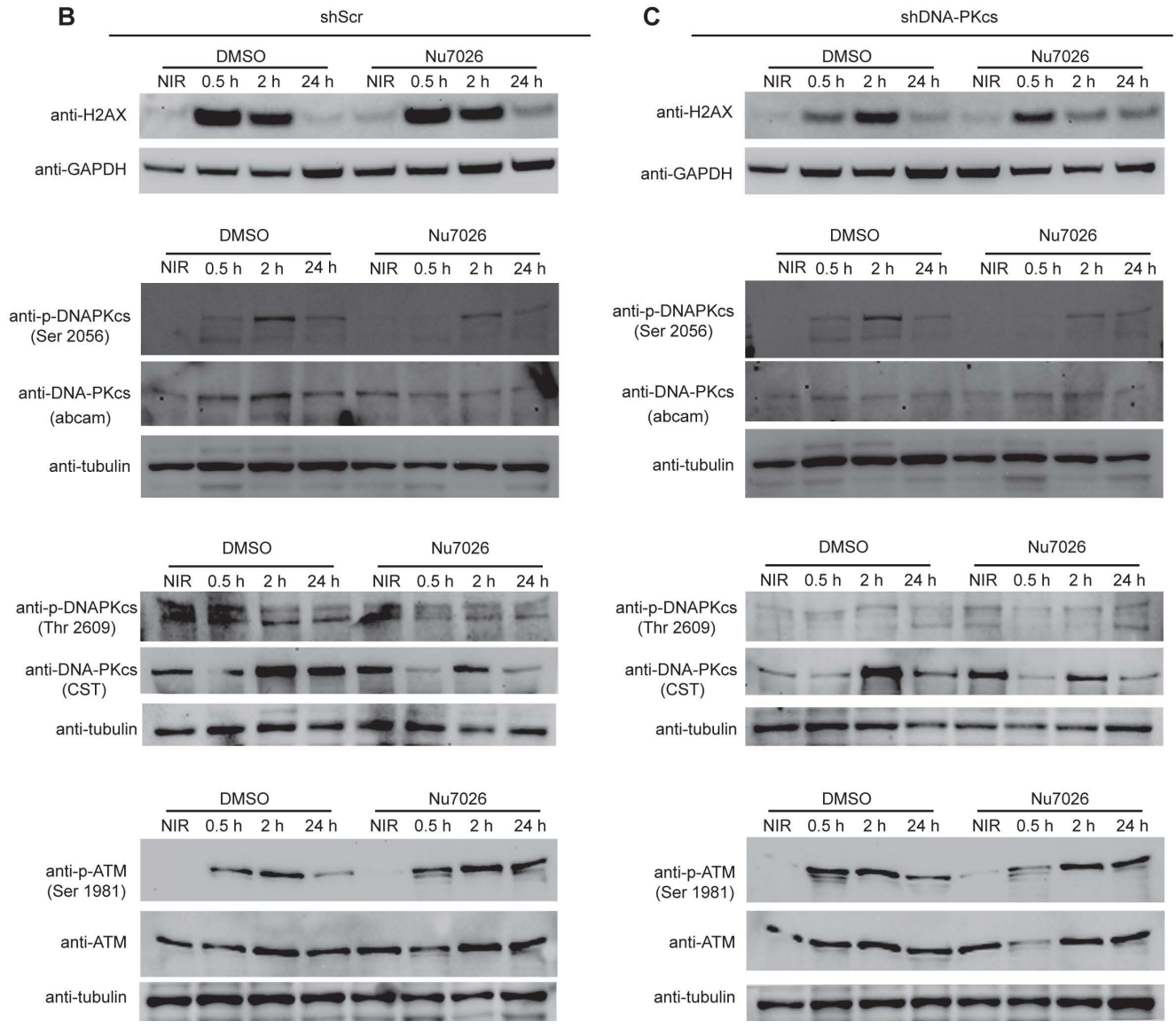

Fig. S1: Western blot analysis of protein expression.

A. Verification of the efficiency of corresponding shRNAs by Western blot. Cells were collected from passage 2 or 3 after selection with puromycin and whole cell lysates were extracted. **B, C.** Western blot for corresponding proteins in the presence or absence of Nu7026 (10 μM) in response to irradiation. shScr (**B**) and shDNA-PKcs (**C**) were treated with DMSO or Nu7026 (10 μM) 1 h before 6 Gy. Cell lysate was collected at the indicated time points. Approximately 70 μg total protein was loaded into each lane.

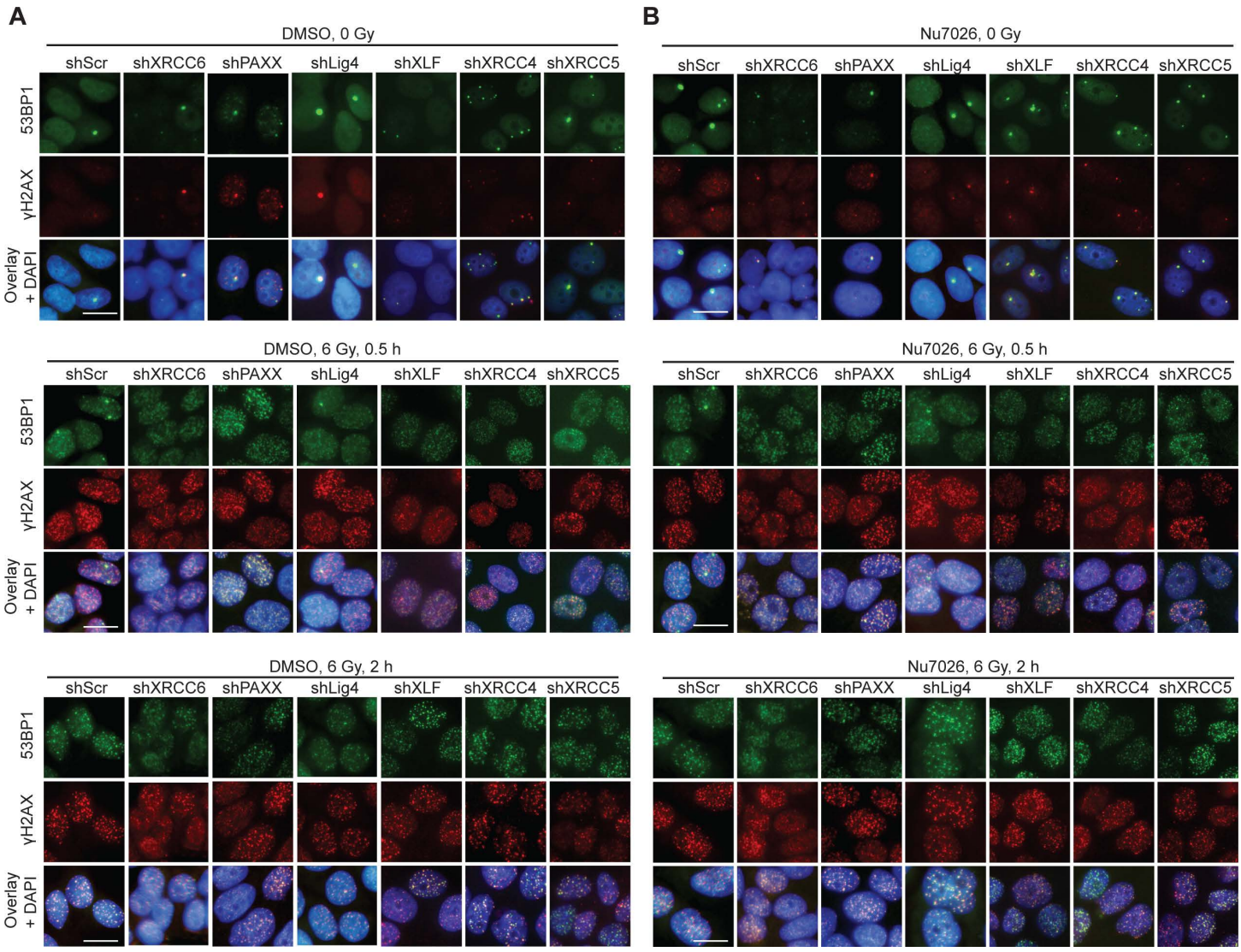

Fig. S2: DNA-PKcs inhibitor Nu7026 does not alter foci formation in cells expressing shRNAs targeting NHEJ repair factors.

A, B. Immunofluorescence analysis of γH2AX and 53BP1. shScr and shNHEJ were treated with DMSO (**A**) or Nu7026 (10 μM) (**B**)1 h before 6 Gy. Cells were stained at indicated time points after radiation with anti-53BP1 (green) or anti-γH2AX (red). Three color overlay with DAPI (blue) shown for representative examples. Scale bar = 20 μm.

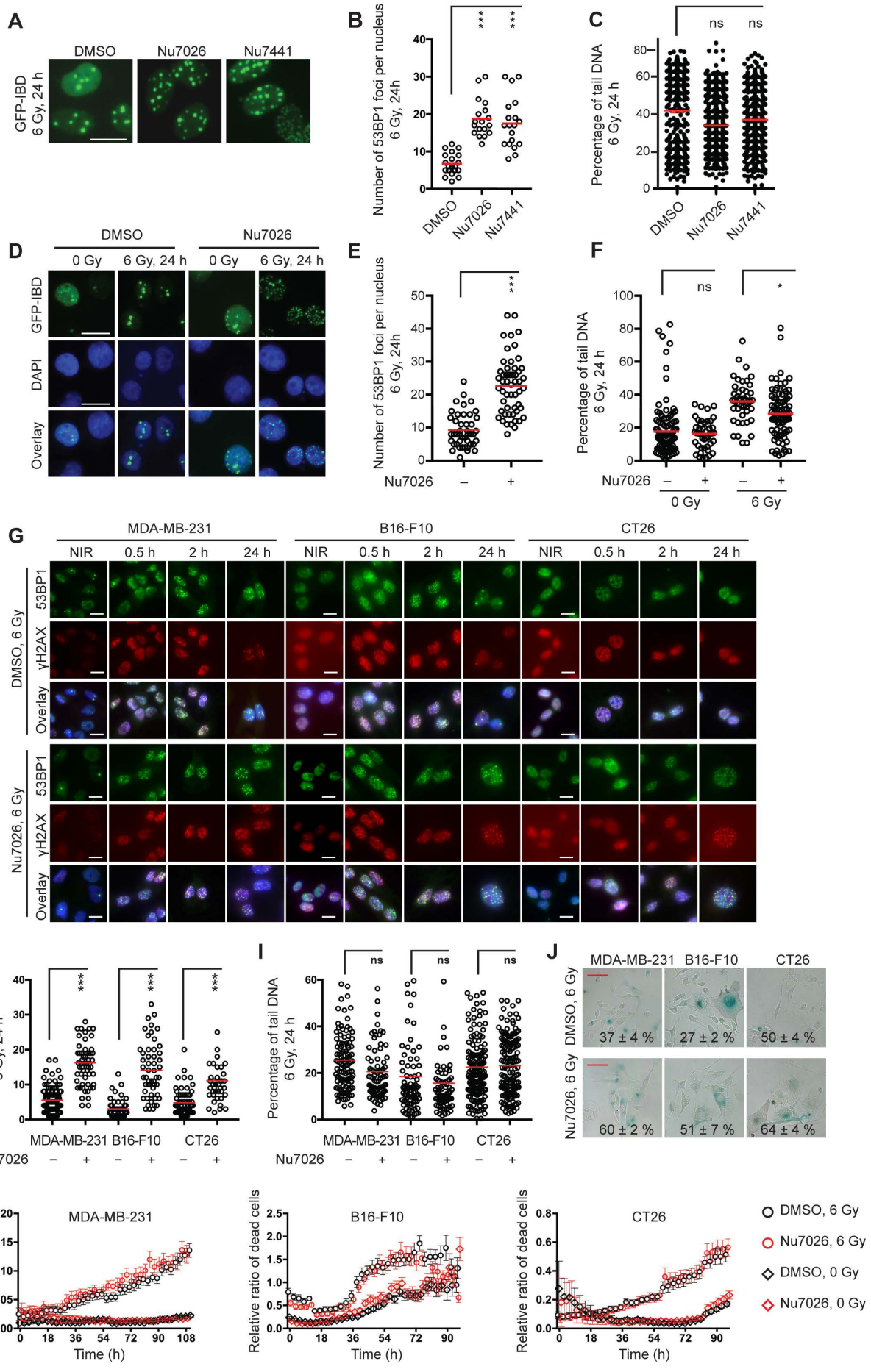

Fig. S3: The effect of DNA-PKcs deficiency on foci resolution is not a cell-type- or inhibitor-specific phenotype.

A. Fluorescence imaging of GFP-IBD foci in MCF7 cells. MCF7 cells were treated with DMSO, Nu7026 (10 μM) or Nu7441 (1 μM) 1 h before 6 Gy. Representative images are shown at 24 h after irradiation. Scale bar = 20 μm. **B.** Quantification of GFP-IBD foci as in **A**. N > 20 cells, mean ± s.d. (red bar). **C.** Quantitative analysis of DSBs in MCF7 cells detected by neutral comet assay after treatment as in **A.** Cells were collected 24 h after 6 Gy. N > 100. **D**. Live-cell fluorescence imaging of GFP-IBD reporter for 53BP1 in MDA-MB-435 cells. MDA-MB-435$^{GFP\text{-}IBD}$ cells were treated with DNA-PKcs inhibitor Nu7026 (10 μM) 1 h before IR and images captured 24 h after 0 or 6 Gy. Representative images are shown. Scale bar = 20 μm. **E.** Quantification of GFP-IBD foci as in **D** at 24 h. N > 50 cells, mean ± s.d. (red bar). **F.** Quantitative analysis of DSBs in MDA-MB-435 cells by neutral comet assay after treatment with DMSO or Nu7026 (10 μM)1 h before 0 or 6 Gy. Cells were collected 24 h after 6 Gy. **G.** Immunofluorescence analysis of γH2AX and 53BP1. MDA-MB-231, B16-F10, and CT26 cells were treated with DMSO or Nu7026 (10 μM) 1 h before 6 Gy. Cells were stained at the indicated time points after radiation with anti-53BP1 (green) or anti-γH2AX (red). Three color overlay with DAPI (blue) shown for representative examples. Scale bar = 20 μm. **H.** Quantification of 53BP1 foci as in **G** at 24 h. N > 100 cells, mean ± s.d. (red bar). **I**. Quantitative analysis of DSBs in MDA-MB-231, B16-F10, and CT26 cells by neutral comet assay after treatment with DMSO or Nu7026 (10 μM)1 h before 6 Gy. Cells were collected 24 h after 6 Gy. N > 100 cells, mean ± s.d. (red bar). **J.** SA-βGal staining in indicated cells. Cells were treated as in **I** and stained 5 d after 6 Gy. At least 5 images were captured with randomly selected, non-overlapping fields. Representative images are shown. Mean percentage of SA-βGal^{+} cells ± s.d. from five 20X fields indicated. Scale bar = 200 μm. **K.** Growth curve of indicated cells. Cell were treated as in **I**. Cell growth was recorded by IncuCyte S3 immediately after 6 Gy for 4 d. Unpaired t-test compared to DMSO controls, ***, $p < 0.001$; *, $p < 0.05$; ns, $p > 0.05$.

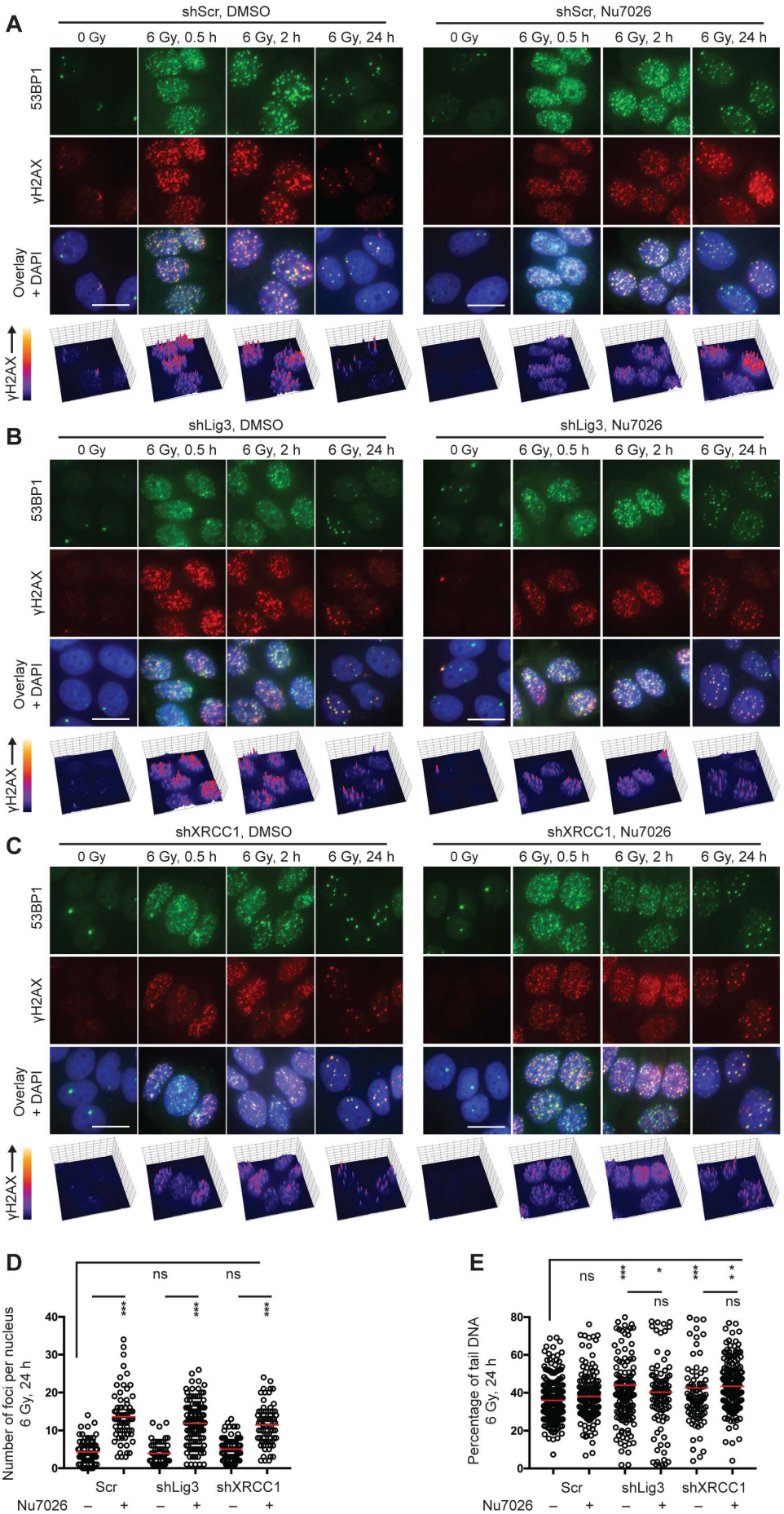

Fig. S4: Inhibition of DNA-PKcs induces persistent foci without further delaying DSB repair in cells with alt-EJ defects.

A, B and **C**, Immunofluorescence analysis of γH2AX and 53BP1. shScr (**A**) control and shLig3 (**B**) and shXRCC1 (**C**) targeting alt-EJ were treated with Nu7026 (10 μM) 1 h before 6 Gy. At indicated time points after irradiation, cells were analyzed for foci with anti-53BP1 (green) or anti-γH2AX (red), shown as three color overlay with DAPI (blue) and perspective plots of γH2AX staining intensity for representative examples from each condition. Scale bar = 20 μm. **D.** Quantification of γH2AX foci as in **A, B** and **C** at 24 h after 6 Gy. N > 100 cells, mean ± s.d. (red bar). Unpaired t-tests compared to non-Nu7026 controls, ***, $p < 0.001$. **E.** Quantitative analysis of DSBs in MCF7 cells by neutral comet assay after treatment as in **A.** Cells were collected 24 h after 6 Gy. N > 100 cells, mean ± s.d. (red bar). Unpaired t-tests compared to DMSO controls, ***, $p < 0.001$; **, $p < 0.01$.

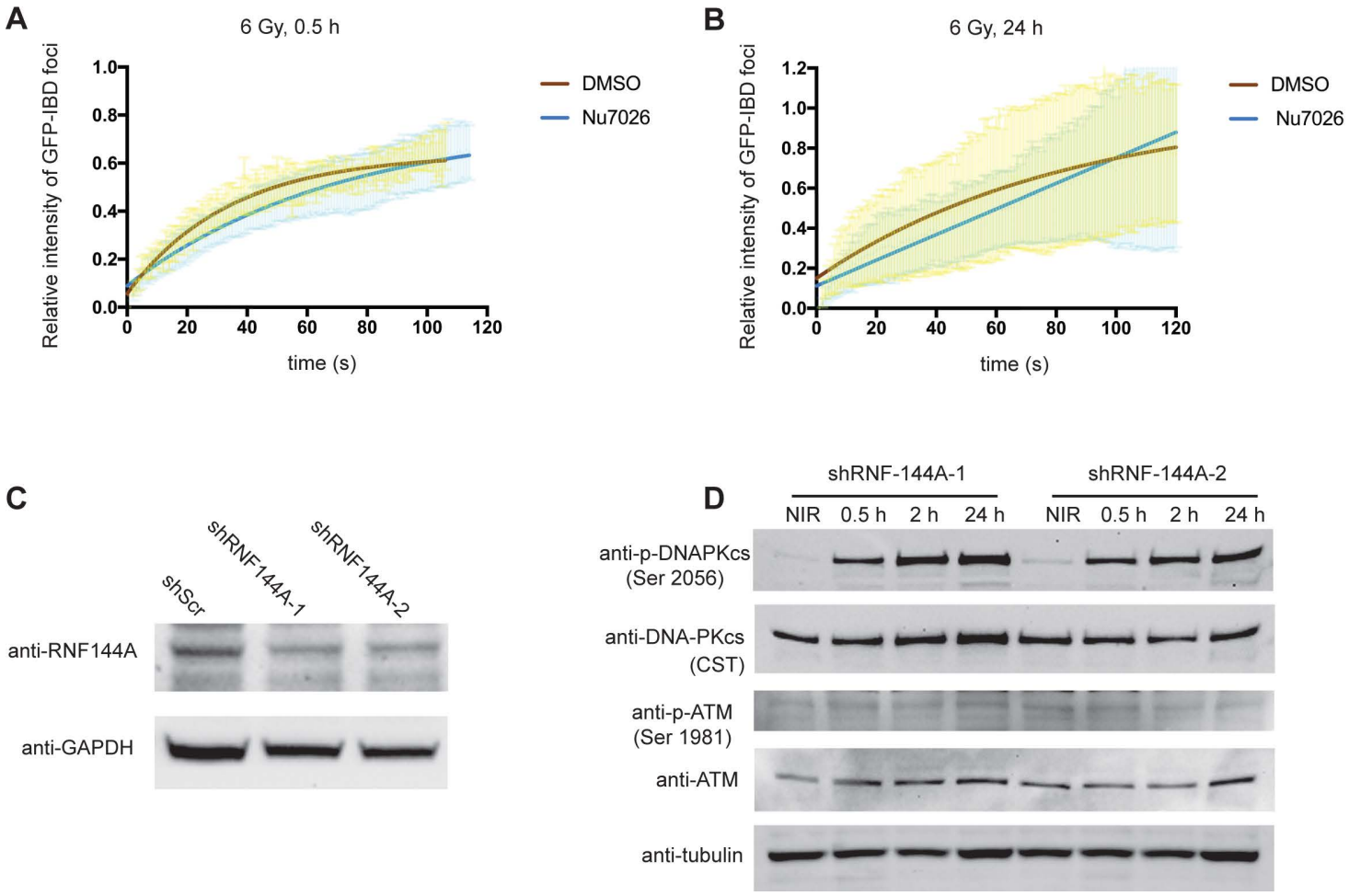

Fig. S5: Fluorescence recovery after photobleach (FRAP) analysis of molecular exchange in GFP-IBD foci and the effect of shRNF-144A on DNA-PKcs and ATM in response to irradiation.

A, B. Fluorescence recovery after photobleach (FRAP) analysis of molecular exchange of the GFP-IBD reporter in foci formed in MCF7$^{GFP\text{-}IBD}$ cells treated with Nu7026 (10 μM) or DMSO 1 h before 6 Gy and examined at 0.5 h (**A**) and 24 h (**B**) after irradiation, representing newly formed and persistent foci respectively. Data were fitted with easyFRAP. N > 10 foci, mean (solid line) ± s.d. **C.** Western blot validation of shRNF-144A. Two shRNA-144A constructs were used. **D.** Western blot analysis of the indicated proteins in shRNF-144A cells after 6 Gy. Cell lysate was collected at the indicated time points. Approximately 70 μg total protein was loaded for each sample.

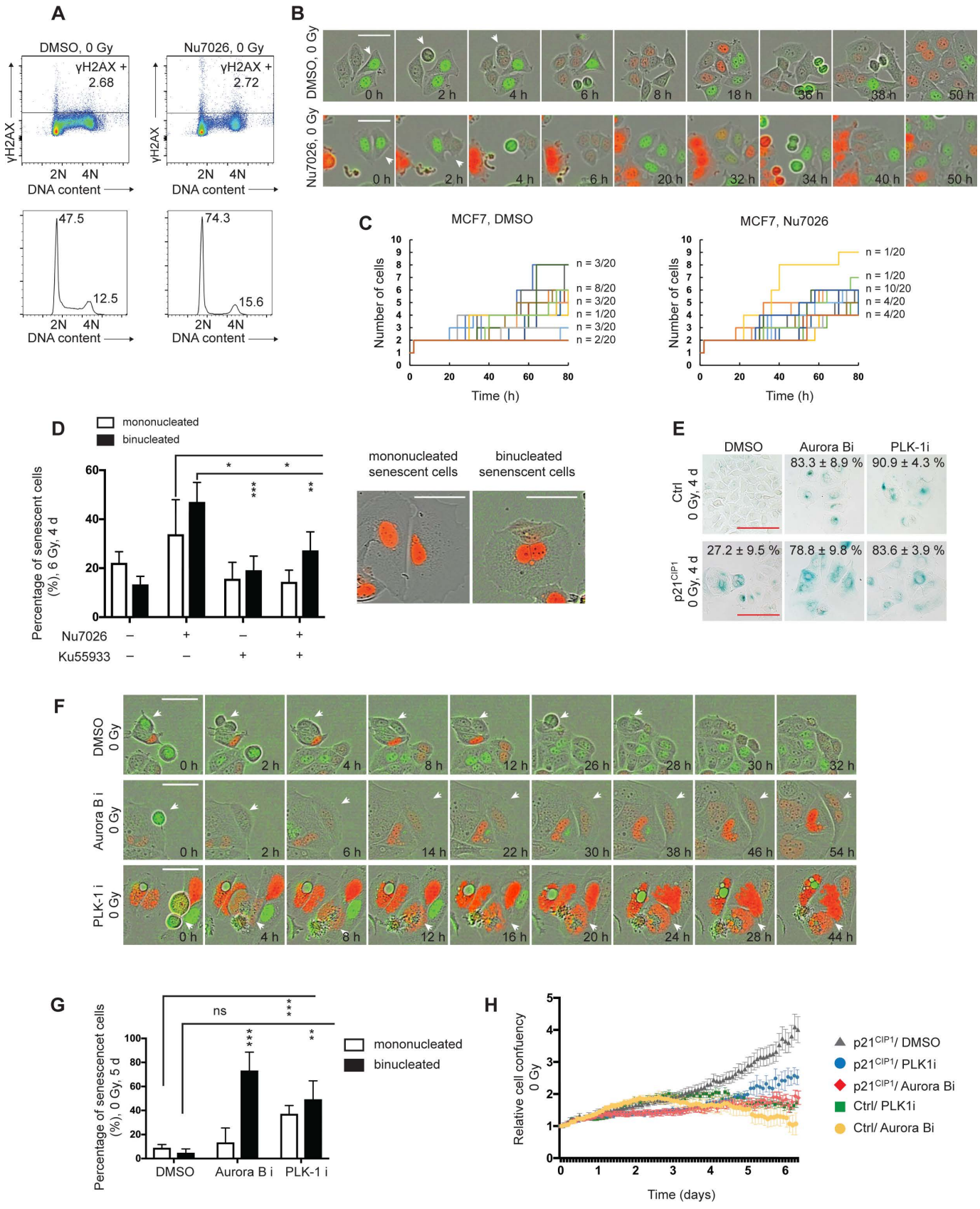

Fig. S6: Tracking of cell behaviors after treatments.

A. Flow cytometry analysis of DNA content (DAPI) and γH2AX in cells treated with DMSO or Nu7026 (10 μM) and then collected after 24 h. The 2D dot plots (upper) show γH2AX staining across the cell cycle. The gate for γH2AX$^+$ was set based these unirradiated cell sample. The histograms (lower) show relative abundance at each DNA content. Data acquired from 50,000 cells per sample. **B.** Time-lapse analysis of MCF7-FUCCI cells treated with DMSO or Nu7026 (3 μM) for 24 h before imaging. Representative cells shown at indicated times. Carets indicate cells that perform mitosis and cytokinesis during time course. Scale bar = 50 μm. **C.** Tracking cell division of single cells. MCF7 cells were treated as in **B**. The time at which rounding up for mitosis was first observed was set as 0 h. Then, 20 cells were tracked for each condition, revealing distinct trajectories of completed cell division and/or mitotic slippage. **D.** ATM inhibitor Ku55933 partially rescues mitotic slippage caused by Nu7026 after 6 Gy. (Left) Analysis of senescent morphology in MFC7 cells treated with DMSO, Nu7026 (3 μM), Ku55933 (0.3 μM) or the combination for 1 h before 6 Gy and tracked by time-lapse recording. More than 50 cells from 10 randomly captured, non-overlapping images, were tracked for 4 d after irradiation. Cells with senescent morphology were classified as mono- or binucleated. Histogram shows mean ± s.d. **E.** SA-βGal staining in MCF7 cells. MCF7 control (Ctrl) or p21^{CIPI} overexpression (p21) cells were treated with DMSO, Aurora B inhibitor or PLK-1 inhibitor and stained after 4 d. At least 5 images were captured from randomly selected, non-overlapping fields. Representative images are shown. Mean percentage of SA-βGal$^+$ cells ± s.d. from five 20x fields indicated. Scale bar = 200 μm. **F.** Time-lapse analysis of MCF7-FUCCI cells treated with DMSO, Aurora B inhibitor (Aurora B i) or PLK-1 inhibitor (PLK-1 i). Representative cells shown at indicated times. Carets indicate cells that performed mitosis and cytokinesis during the time course. Scale bar = 50 μm. **G.** Analysis of senescent morphology in MCF7 cells treated as in **F**. More than 50 cells from 10 randomly captured, non-overlapping images, were tracked to 5 d after irradiation. Cells with senescent morphology were classified as mono- or binucleated. Histogram shows mean ± s.d. for each condition. **H**, Automated proliferation analysis from time-lapse imaging over 6 d comparing control (Ctrl) or p21^{CIPI} overexpression (p21) cells treated with DMSO, Aurora B inhibitor or PLK-1 inhibitor. For statistical analysis, unpaired t-test, **, $p < 0.01$; ***, $p < 0.001$. (Right) Diagram represents mononucleated or binucleated senescent cells. Scale bar = 50 μm.

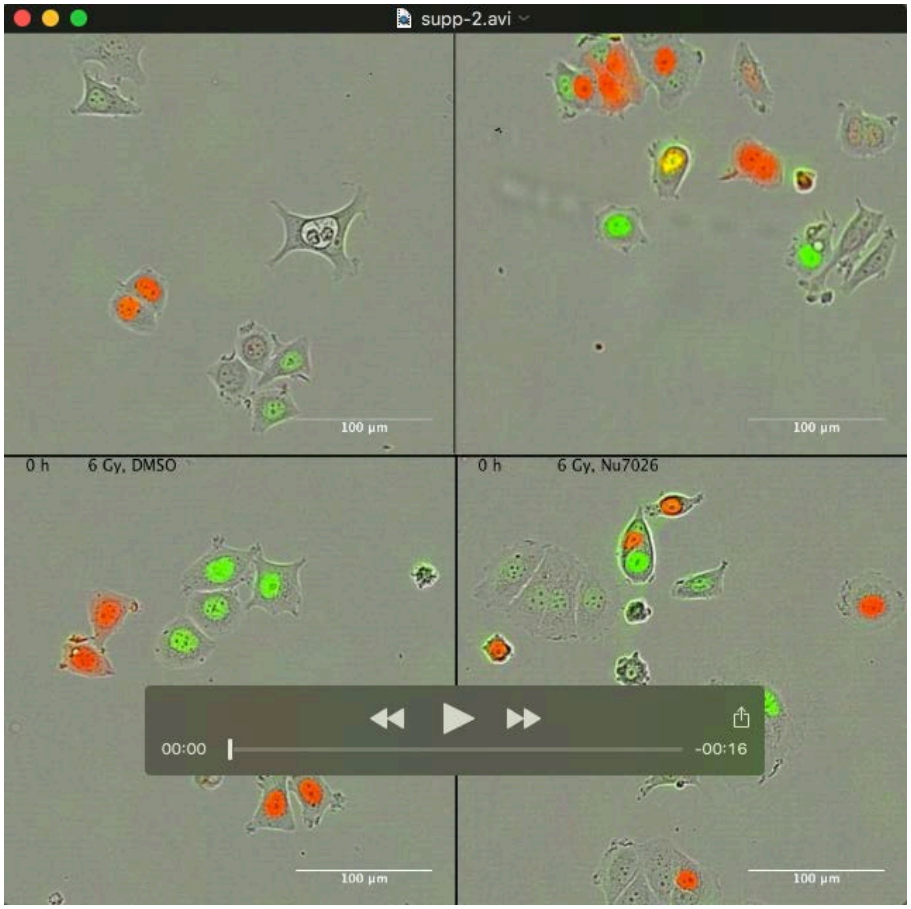

Movie 1. DNA-PKcs inhibitor Nu7026 induces mitotic slippage after irradiation, related to Figure 7 and Figure S5.

Time-lapse imaging of MCF7-FUCCI cells treated with DMSO or Nu7026 (3 µM) following 6 Gy irradiation or not. Cells were treated with DMSO or Nu7026 (3 µM) for 1 h, irradiated with 0 Gy or 6 Gy and then images were taken at 2 h intervals. Following 0 Gy, most of the cells underwent normal mitosis in which parent cells divided into two separated daughter cells approximately every 24 h in the presence or absence of Nu7026. Following 6 Gy, though some of the surviving cells treated with DMSO recovered from irradiation after a few cell cycles, others lost the capability for cell division and accumulate as flattened and enlarged cells displaying characteristic senescent morphology. However, many surviving cells with Nu7026 treatment entered the cell cycle but failed to complete cytokinesis and yielded binucleated cells, which adopted a senescent phenotype over time. Most cells with senescent morphology terminally arrested while expressing mCherry-hCdt1 (red), representing G1 cell cycle stage. Scale bar = 100 µm.

Journal of Cell Science • Supplementary information

Movie 2. ATM inhibitor Ku55933 partially rescues mitotic slippage caused by Nu7026 after 6 Gy, related to Figure 7 and Figure S6.

Time-lapse imaging of MCF7-FUCCI cells treated with Ku55933 (0.3 µM) or the combination of Ku55933 and Nu7026 (3 µM) following 6 Gy. Cells were treated with inhibitors for 1 h, irradiated with 6 Gy and then images were taken at 2 h intervals. In both cases, most surviving cells entered the cell cycle and completed cytokinesis, but many did not progress further. A high proportion of these daughters contained micronuclei and died instead of continuing on to senescence. Scale bar = 100 µm.

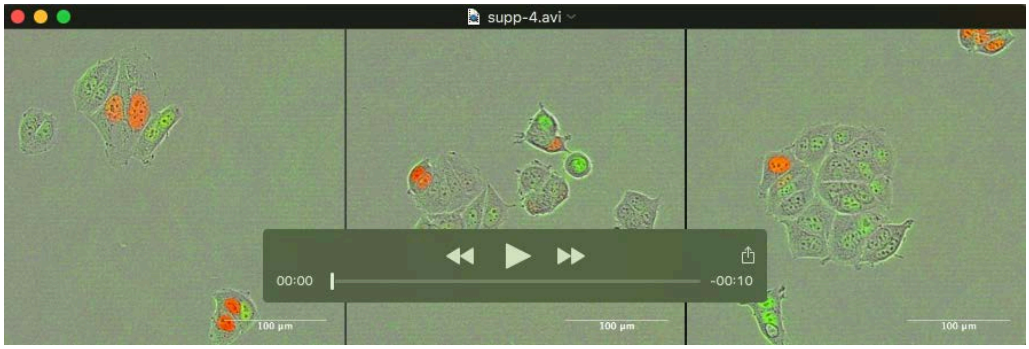

Movie 3. Mitosis and/or cytokinesis defects in unirradiated cells is sufficient to promote accelerated senescence, related to Figure 7 and Figure S7.

Time-lapse imaging of MCF7-FUCCI cells treated with DMSO, Aurora B kinase inhibitor, or PLK-1 inhibitor. Images were taken at 2 h intervals beginning 1 h after inhibitors treatment. With DMSO treatment, most of the cells underwent normal mitosis in which cell divided approximately every 24 h. With Aurora B kinase or PLK-1 inhibitor treatment, cells underwent mitotic slippage and/or catastrophe. Though many cells died, surviving cells eventually displayed senescent phenotype with mCherry-hCdt1 (red, G1) expression. Scale bar = 100 µm.

Movie 4. Overexpression of p21^{CIP1}rescues cell death induced by Aurora B or PLK1 inhibitors and yields homogeneous senescence, related to Figure 7 and Figure S7.

Time-lapse imaging of MCF7-FUCCI or p21^{CIPI} overexpression (p21) cells treated with DMSO, Aurora B or PLK1 inhibitors. Images were taken at 2 h intervals beginning 1 h after inhibitors treatment. In MCF7 cells with DMSO treatment, most of cells underwent cell cycle every 24 h. In MCF7 cells treated with Aurora B or PLK1 inhibitors, cells displayed mitotic slippage and some cells developed senescent morphology while some binucleate cells died rather than entering senescence. P21 overexpression can induce senescence on its own but when combined with the Aurora B or PLK1 inhibitors, the binucleate cells were rescued from death, yielding nearly homogeneous senescence.

Journal of Cell Science • Supplementary information

Table S1. List of chemical probes and their working concentrations.

Chemical probe	Targeted protein	Company	Catalog #	Working concentration
Nu7026	DNA-PKcs	Selleckchem	S2893	10 μM
Ku55933	ATM	Selleckchem	S1092	5 μM
CHIR124	Chk1	Cayman	16553	0.5 μM
Chk2 inhibitor	Chk2	Cayman	17552	5 μM
MK-8745	Aurora A	MedChem Express	HY-13819	1 μM
AZD1152-HQPA	Aurora B	MedChem Express	10126	0.5 μM
GSK461364	PLK-1	MedChem Express	50877	0.5 μM

Table S2. List of shRNAs.

Targeted protein	Sigma MISSION shRNA Catalog #	shRNA sequence
DNA-PKcs (PRKDC)(a)	TRCN0000195491	CCGGCCTCCAGGTTAGGATTAATTGCTCGAGCAATTAATCCTAACC TGGAGGTTTTTTG
DNA-PKcs (PRKDC)(b)	TRCN0000194719	CCGGCCTGAAGTCTTTACAACATATCTCGAGATATGTTGTAAAGAC TTCAGGTTTTTTG
ATM(a)	TRCN0000039948	CCGGCCTTTCATTCAGCCTTTAGAACTCGAGTTCTAAAGGCTGAAT GAAAGGTTTTTG
ATM (b)	TRCN0000039951	CCGGGCCTCCAATTCTTCACAGTAACTCGAGTTACTGGAAGAATTG GAGGTTTTTG
XRCC4 (a)	TRCN0000040117	CCGGCCTCAGGAGAATCAGCTTCAACTCGAGTTGAAGCTGATTCT C CTGAGGTTTTTG
XRCC4 (b)	TRCN0000009875	CCGGTGTGTGAGTGCTAAGGAAGCTCTCGAGAGCTTCCTTAGCAC T CACACATTTTTG
XRCC5(a)	TRCN0000295856	CCGGAGAGGAAGCCTCTGGAAGTTCCTCGAGGAACTTCCAGAGG C TTCCTCTTTTTTG
XRCC5(b)	TRCN0000307986	CCGGAATCTAAGAGAGCTGCCATCGCTCGAGCGATGGCAGCTCT C TTAGATTTTTTTG
XRCC6 (a)	TRCN0000039608	CCGGCGACATAAGTCGAGGGACTTTCTCGAGAAAGTCCCTCGAC T TATGTCGTTTTTG
XLF (a)	TRCN0000275632	CCGGTACCATGGACTTTAGGTATATCTCGAGATATACCTAAAGTCC ATGGTATTTTTG
XLF (b)	TRCN0000275628	CCGGGCTAGCAACGTTACTTCATATCTCGAGATATGAAGTAACGTT GCTAGCTTTTTG
PAXX(C9orf142)(a)	TRCN0000263653	CCGGCTCTTCTTACCAGACCCAGATCTCGAGATCTGGGTCTGGTA A GAAGAGTTTTTG
PAXX(C9orf142)(b)	TRCN0000263654	CCGGACAGAGCATCCCTGACGCTTTCTCGAGAAAGCGTCAGGGA T GCTCTGTTTTTTG
Ligase4(a)	TRCN0000040004	CCGGGCCCGTGAATATGATTGCTATCTCGAGATAGCAATCATATTC ACGGGCTTTTTG
Ligase4(b)	TRCN0000040005	CCGGGCTCGCATCTAAACACCTTTACTCGAGTAAAGGTGTTTAGAT GCGAGCTTTTTG
RNF144A(a)	TRCN0000004413	CCGGGAACGAGATTGAGTGCATGGTCTCGAGACCATGCACTCAA T CTCGTTCTTTTT
RNF144A(b)	TRCN0000421486	CCGGATGTTGAGCTCTTGATCAAAGCTCGAGCTTTGATCAAGAGC T CAACATTTTTTTG
XRCC1(a)	TRCN0000007912	CCGGCCTTCTGGTCACCTCATCTTTCTCGAGAAAGATGAGGTGACC A GAAGGTTTTT
XRCC1(b)	TRCN0000007913	CCGGCCAGTGCTCCAGGAAGATATACTCGAGTATATCTTCCTGGAG C ACTGGTTTTT
Ligase3(a)	TRCN0000048499	CCGGCCGGATCATGTTCTCAGAAATCTCGAGATTTCTGAGAACATGA TCCGGTTTTTG
Ligase3(b)	TRCN0000048500	CCGGGCTGAGTAACTCCAACAGCAACTCGAGTTGCTGTTGGAGTT A CTCAGCTTTTTG

Table S3. List of antibodies.

Antibody/protein	Company	Catalog #	Dilution
γ-H2AX, clone JBW301	EMD Millipore	05-636	1:1000
γ-H2AX(Alexa 647 conjugate)	Cell Signaling Technology	9720	1:50
γ-H2AX	Cell Signaling Technology	9718	1:1000
53BP1	Novus	NB100-304	1:1000
DNA-PKcs	Abcam	ab32566	1:500
DNA-PKcs	Cell Signaling Technology	12311	1:1000
DNA-PKcs (Phospho T2609)	Abcam	ab97611	1:500
DNA-PKcs (Phospho S2056)	Abcam	ab124918	1:1000
ATM	Abcam	ab78	1:200
ATM	Cell Signaling Technology	2873	1:1000
ATM (Phospho S1981)	Cell Signaling Technology	4526	1:1000
XRCC5	Abcam	ab80592	1:1000
Ku80	Cell Signaling Technology	2180	1:1000
XRCC6	Abcam	ab202022	1:1000
XRCC4	Abcam	ab97351	1:1000
PAXX	Abcam	ab126353	1:1000
XLF	Abcam	ab33499	1:1000
Ligase4	Abcam	ab26039	1:800
RNF144A	Abcam	ab89260	1:100
Actin (HRP conjugate)	Proteintech	HRP-60008	1:10000
Tubulin (HRP conjugate)	Proteintech	HRP-66031	1:10000

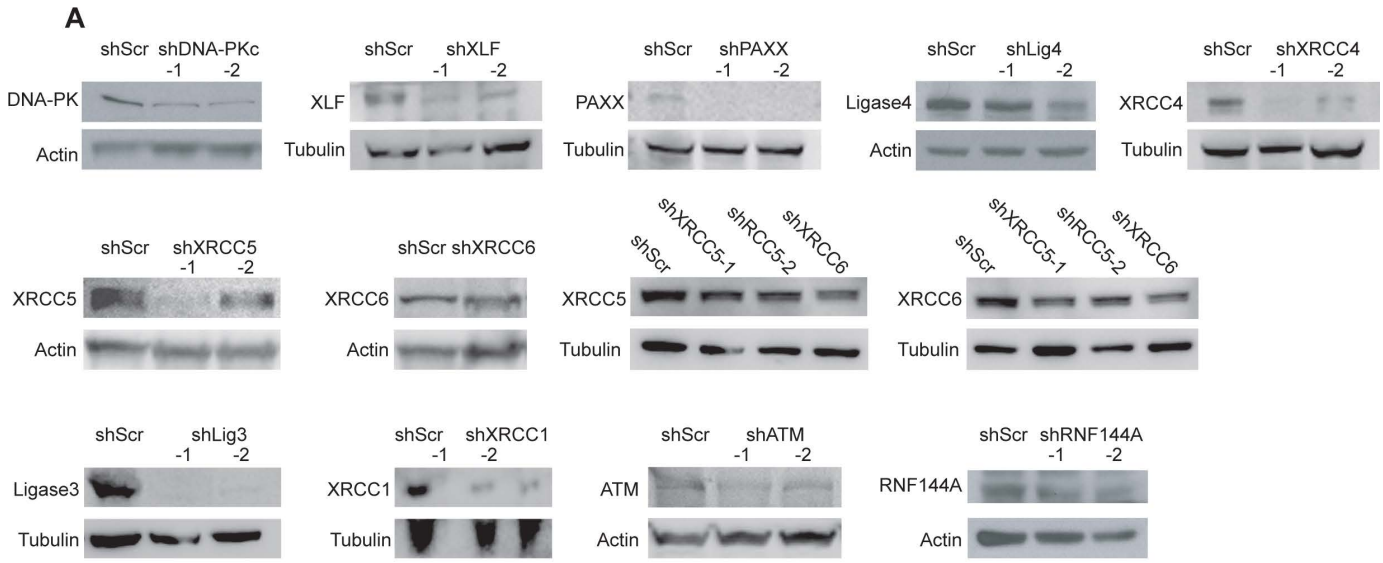

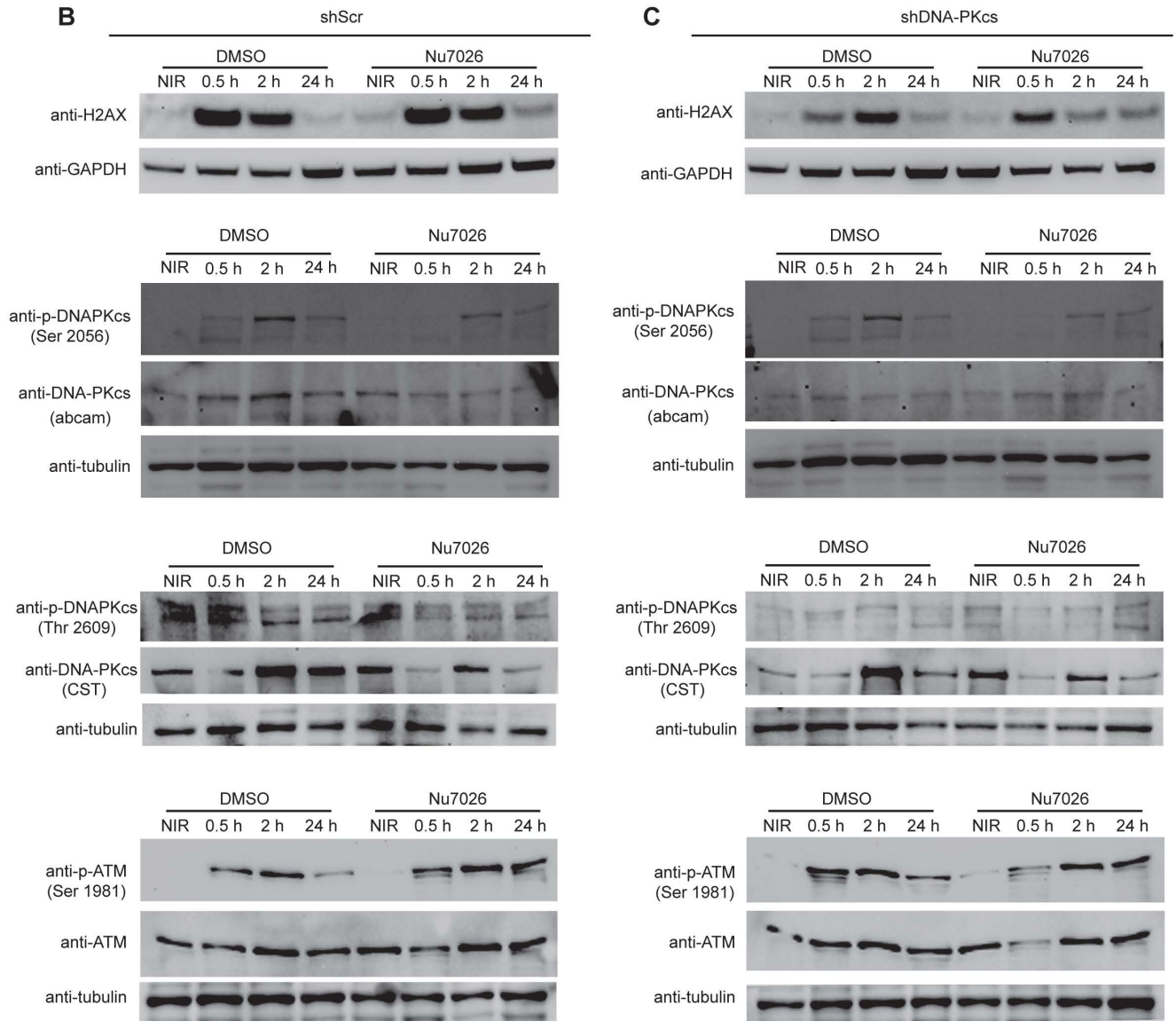

Fig. S1: Western blot analysis of protein expression.

A. Verification of the efficiency of corresponding shRNAs by Western blot. Cells were collected from passage 2 or 3 after selection with puromycin and whole cell lysates were extracted. **B, C.** Western blot for corresponding proteins in the presence or absence of Nu7026 (10 μM) in response to irradiation. shScr (**B**) and shDNA-PKcs (**C**) were treated with DMSO or Nu7026 (10 μM) 1 h before 6 Gy. Cell lysate was collected at the indicated time points. Approximately 70 μg total protein was loaded into each lane.

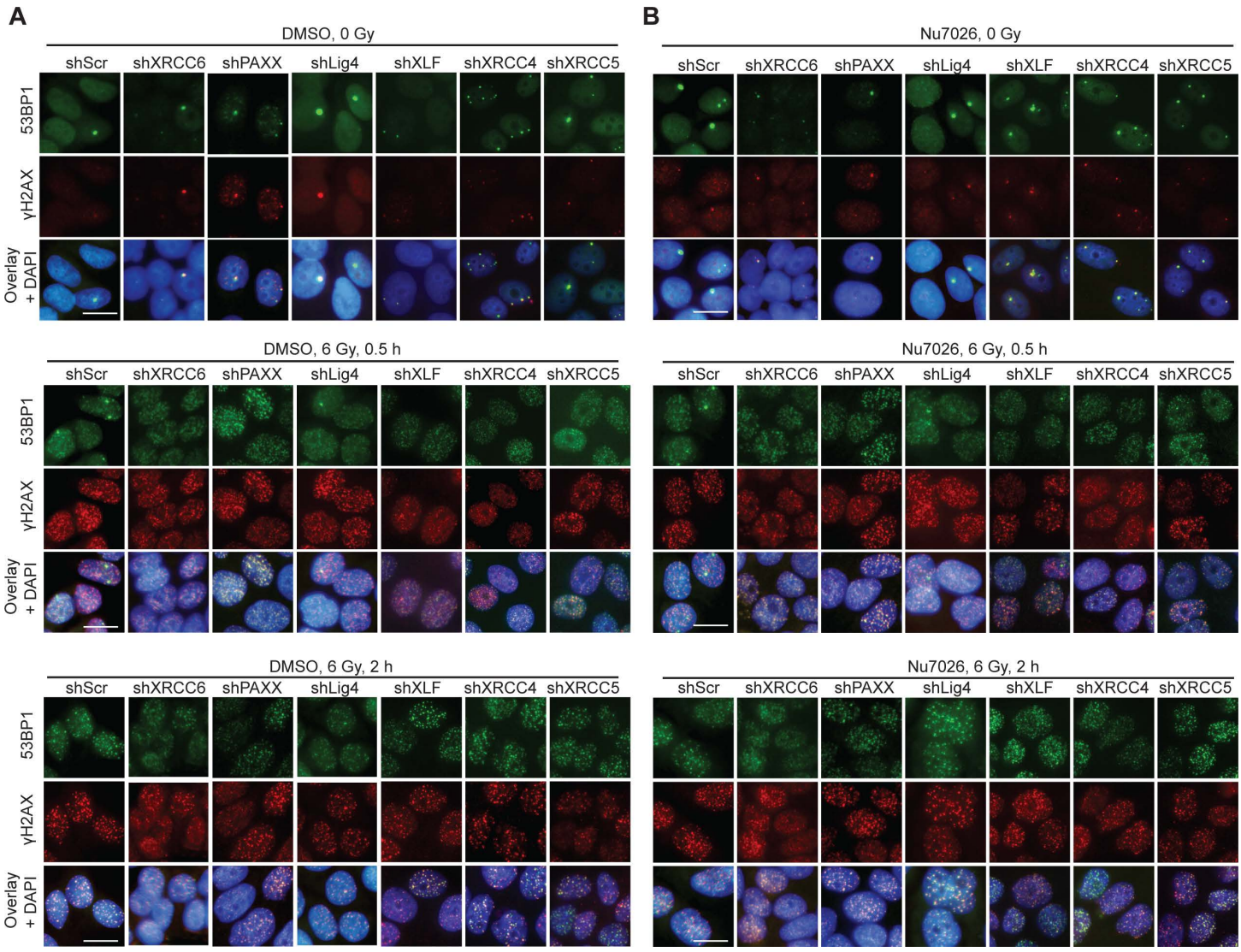

Fig. S2: DNA-PKcs inhibitor Nu7026 does not alter foci formation in cells expressing shRNAs targeting NHEJ repair factors.

A, B. Immunofluorescence analysis of γH2AX and 53BP1. shScr and shNHEJ were treated with DMSO (**A**) or Nu7026 (10 μM) (**B**)1 h before 6 Gy. Cells were stained at indicated time points after radiation with anti-53BP1 (green) or anti-γH2AX (red). Three color overlay with DAPI (blue) shown for representative examples. Scale bar = 20 μm.

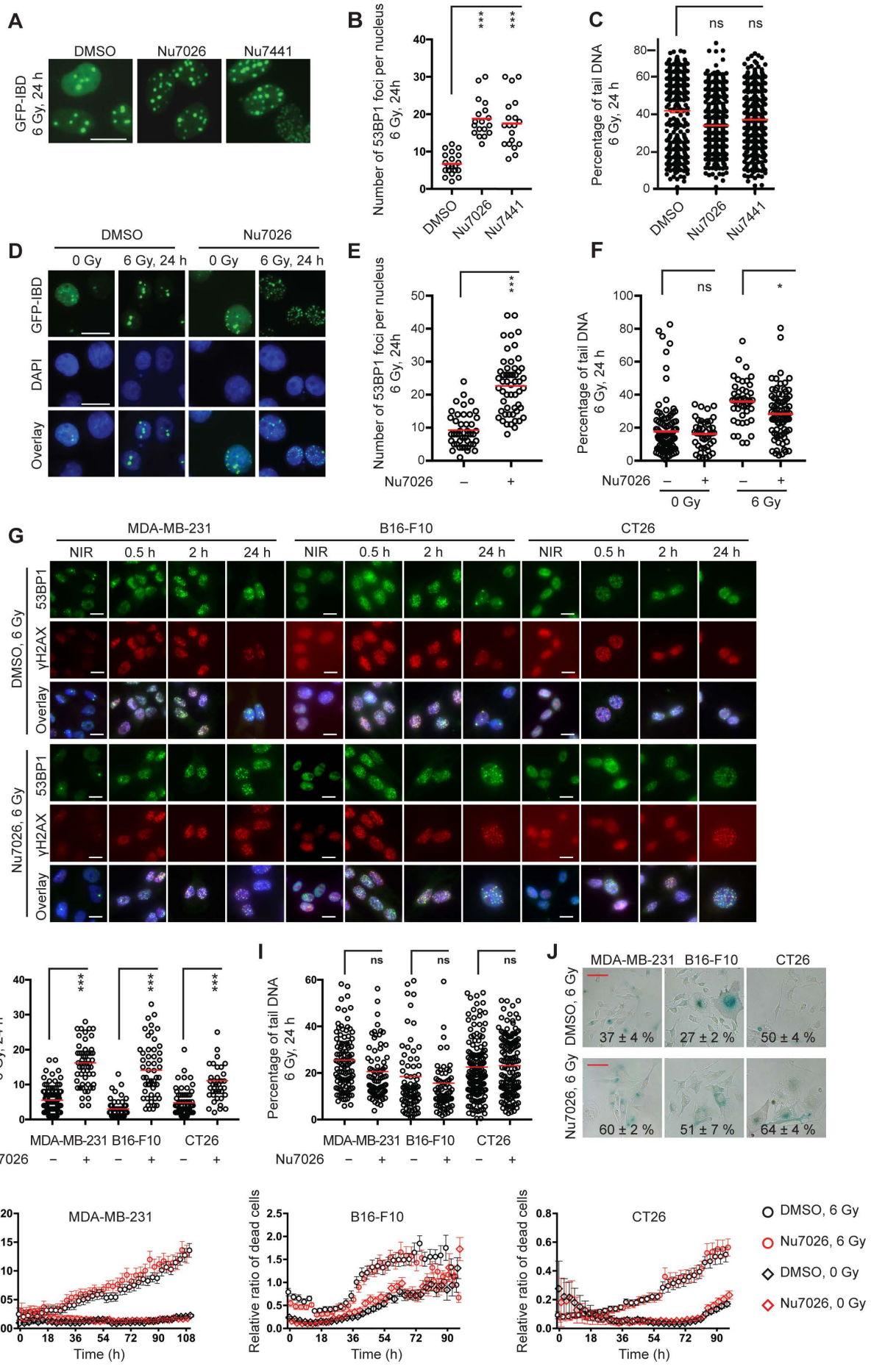

Fig. S3: The effect of DNA-PKcs deficiency on foci resolution is not a cell-type- or inhibitor-specific phenotype.

A. Fluorescence imaging of GFP-IBD foci in MCF7 cells. MCF7 cells were treated with DMSO, Nu7026 (10 μM) or Nu7441 (1 μM) 1 h before 6 Gy. Representative images are shown at 24 h after irradiation. Scale bar = 20 μm. **B.** Quantification of GFP-IBD foci as in **A**. N > 20 cells, mean ± s.d. (red bar). **C.** Quantitative analysis of DSBs in MCF7 cells detected by neutral comet assay after treatment as in **A.** Cells were collected 24 h after 6 Gy. N > 100. **D**. Live-cell fluorescence imaging of GFP-IBD reporter for 53BP1 in MDA-MB-435 cells. MDA-MB-435$^{GFP\text{-}IBD}$ cells were treated with DNA-PKcs inhibitor Nu7026 (10 μM) 1 h before IR and images captured 24 h after 0 or 6 Gy. Representative images are shown. Scale bar = 20 μm. **E.** Quantification of GFP-IBD foci as in **D** at 24 h. N > 50 cells, mean ± s.d. (red bar). **F.** Quantitative analysis of DSBs in MDA-MB-435 cells by neutral comet assay after treatment with DMSO or Nu7026 (10 μM)1 h before 0 or 6 Gy. Cells were collected 24 h after 6 Gy. **G.** Immunofluorescence analysis of γH2AX and 53BP1. MDA-MB-231, B16-F10, and CT26 cells were treated with DMSO or Nu7026 (10 μM) 1 h before 6 Gy. Cells were stained at the indicated time points after radiation with anti-53BP1 (green) or anti-γH2AX (red). Three color overlay with DAPI (blue) shown for representative examples. Scale bar = 20 μm. **H.** Quantification of 53BP1 foci as in **G** at 24 h. N > 100 cells, mean ± s.d. (red bar). **I**. Quantitative analysis of DSBs in MDA-MB-231, B16-F10, and CT26 cells by neutral comet assay after treatment with DMSO or Nu7026 (10 μM)1 h before 6 Gy. Cells were collected 24 h after 6 Gy. N > 100 cells, mean ± s.d. (red bar). **J.** SA-βGal staining in indicated cells. Cells were treated as in **I** and stained 5 d after 6 Gy. At least 5 images were captured with randomly selected, non-overlapping fields. Representative images are shown. Mean percentage of SA-βGal^{+} cells ± s.d. from five 20X fields indicated. Scale bar = 200 μm. **K.** Growth curve of indicated cells. Cell were treated as in **I**. Cell growth was recorded by IncuCyte S3 immediately after 6 Gy for 4 d. Unpaired t-test compared to DMSO controls, ***, $p < 0.001$; *, $p < 0.05$; ns, $p > 0.05$.

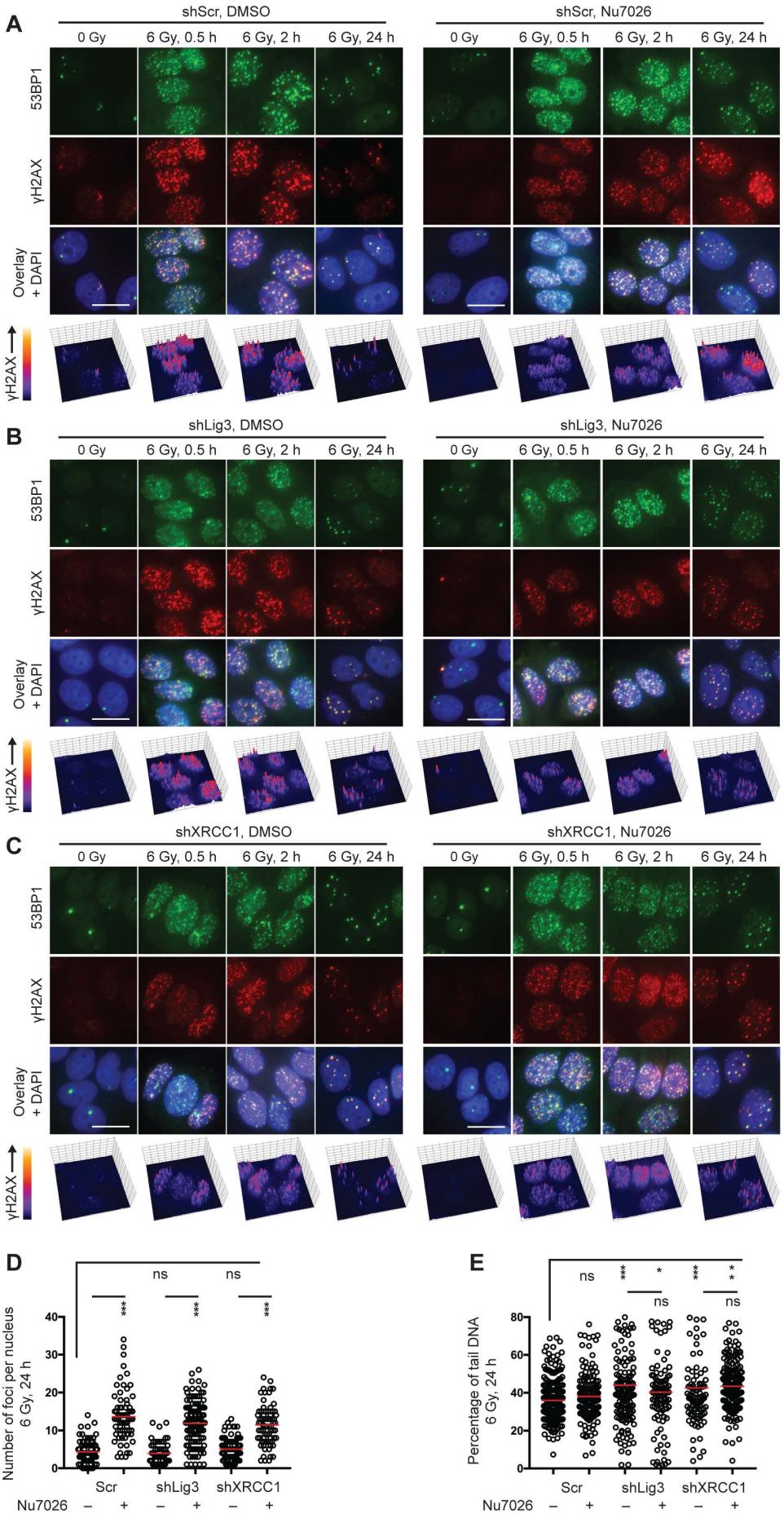

Fig. S4: Inhibition of DNA-PKcs induces persistent foci without further delaying DSB repair in cells with alt-EJ defects.

A, B and **C**, Immunofluorescence analysis of γH2AX and 53BP1. shScr (**A**) control and shLig3 (**B**) and shXRCC1 (**C**) targeting alt-EJ were treated with Nu7026 (10 μM) 1 h before 6 Gy. At indicated time points after irradiation, cells were analyzed for foci with anti-53BP1 (green) or anti-γH2AX (red), shown as three color overlay with DAPI (blue) and perspective plots of γH2AX staining intensity for representative examples from each condition. Scale bar = 20 μm. **D.** Quantification of γH2AX foci as in **A, B** and **C** at 24 h after 6 Gy. N > 100 cells, mean ± s.d. (red bar). Unpaired t-tests compared to non-Nu7026 controls, ***, $p < 0.001$. **E.** Quantitative analysis of DSBs in MCF7 cells by neutral comet assay after treatment as in **A.** Cells were collected 24 h after 6 Gy. N > 100 cells, mean ± s.d. (red bar). Unpaired t-tests compared to DMSO controls, ***, $p < 0.001$; **, $p < 0.01$.

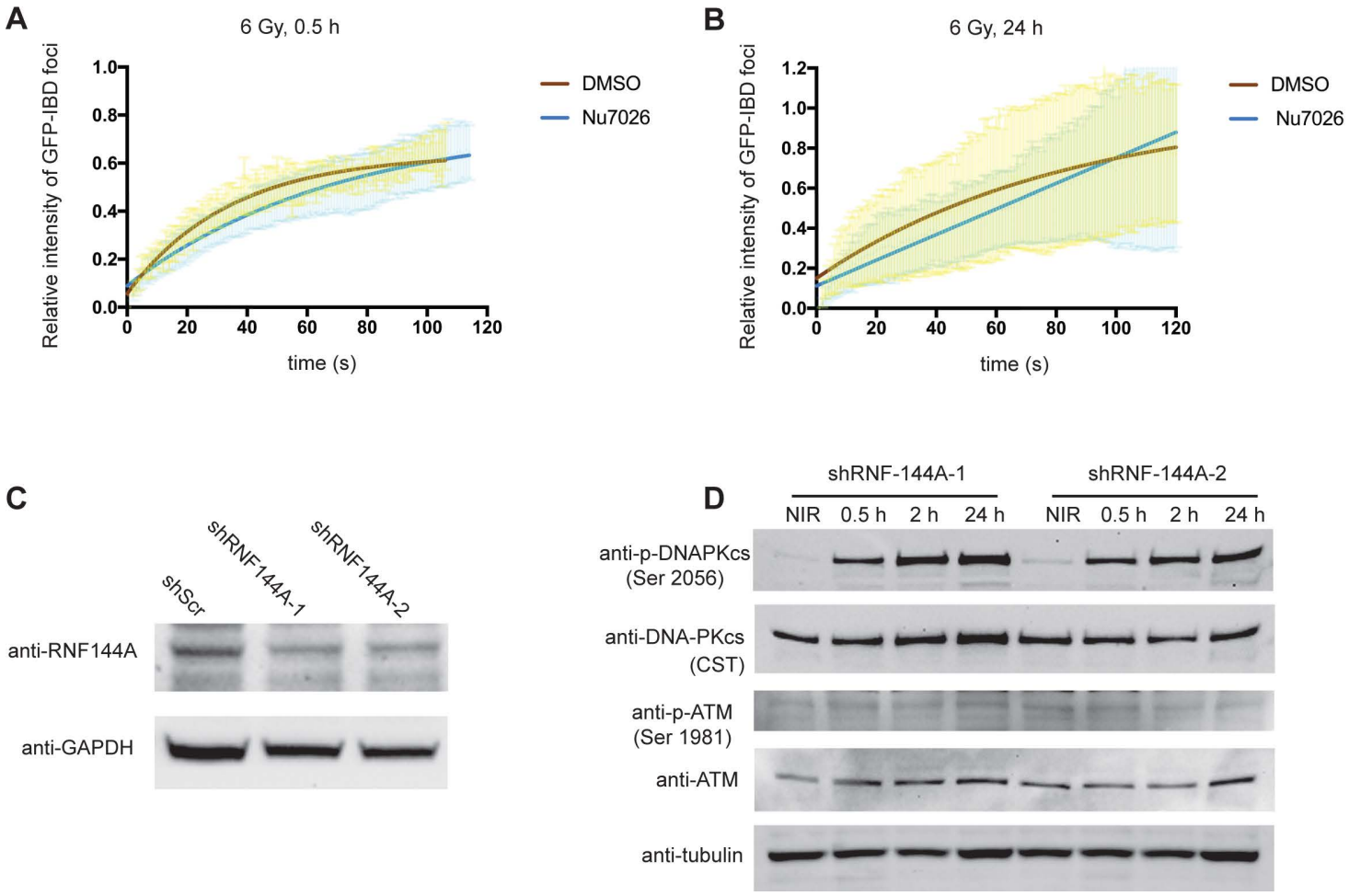

Fig. S5: Fluorescence recovery after photobleach (FRAP) analysis of molecular exchange in GFP-IBD foci and the effect of shRNF-144A on DNA-PKcs and ATM in response to irradiation.

A, B. Fluorescence recovery after photobleach (FRAP) analysis of molecular exchange of the GFP-IBD reporter in foci formed in MCF7$^{GFP\text{-}IBD}$ cells treated with Nu7026 (10 μM) or DMSO 1 h before 6 Gy and examined at 0.5 h (**A**) and 24 h (**B**) after irradiation, representing newly formed and persistent foci respectively. Data were fitted with easyFRAP. N > 10 foci, mean (solid line) ± s.d. **C.** Western blot validation of shRNF-144A. Two shRNA-144A constructs were used. **D.** Western blot analysis of the indicated proteins in shRNF-144A cells after 6 Gy. Cell lysate was collected at the indicated time points. Approximately 70 μg total protein was loaded for each sample.

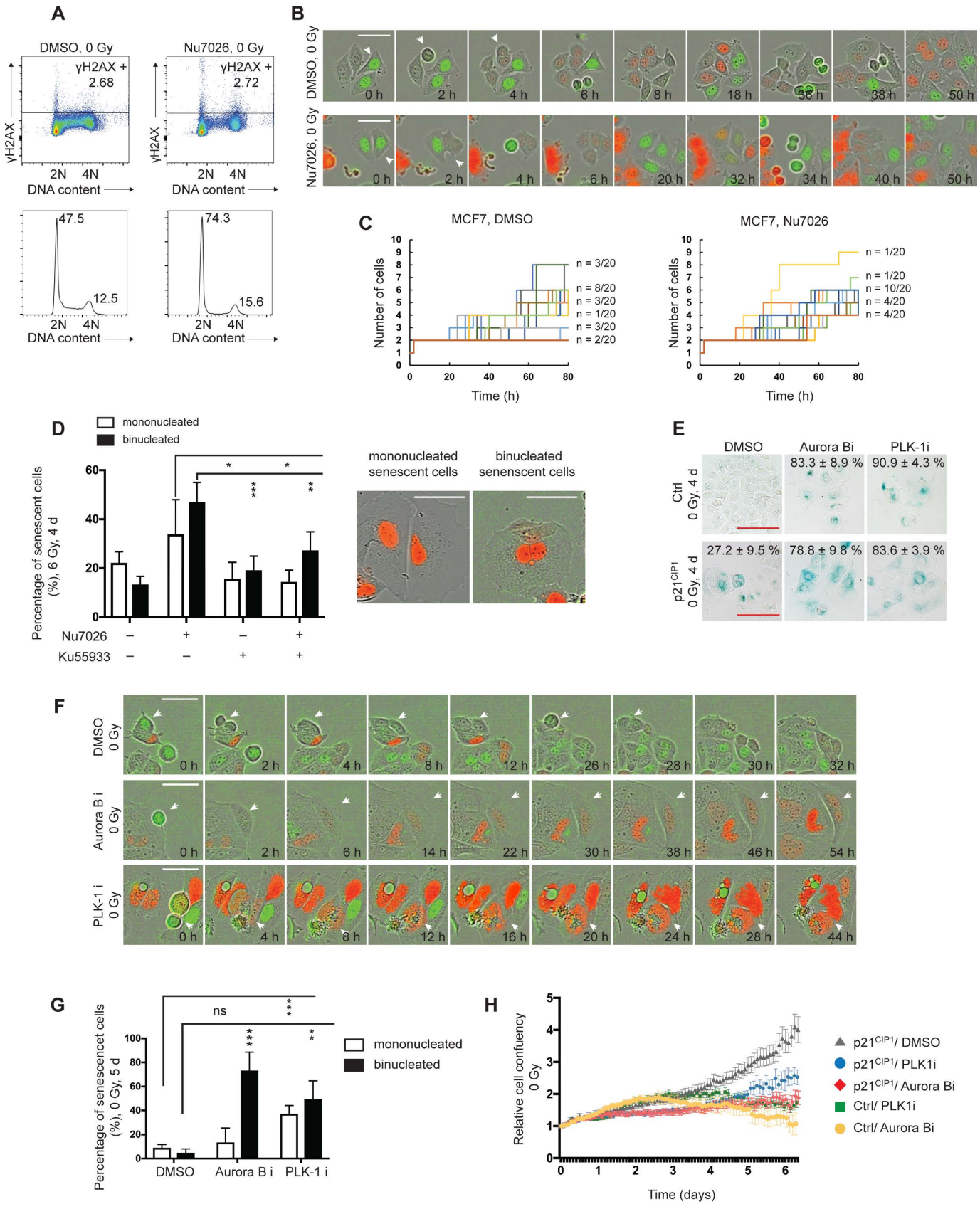

Fig. S6: Tracking of cell behaviors after treatments.

A. Flow cytometry analysis of DNA content (DAPI) and γH2AX in cells treated with DMSO or Nu7026 (10 μM) and then collected after 24 h. The 2D dot plots (upper) show γH2AX staining across the cell cycle. The gate for γH2AX$^+$ was set based these unirradiated cell sample. The histograms (lower) show relative abundance at each DNA content. Data acquired from 50,000 cells per sample. **B.** Time-lapse analysis of MCF7-FUCCI cells treated with DMSO or Nu7026 (3 μM) for 24 h before imaging. Representative cells shown at indicated times. Carets indicate cells that perform mitosis and cytokinesis during time course. Scale bar = 50 μm. **C.** Tracking cell division of single cells. MCF7 cells were treated as in **B**. The time at which rounding up for mitosis was first observed was set as 0 h. Then, 20 cells were tracked for each condition, revealing distinct trajectories of completed cell division and/or mitotic slippage. **D.** ATM inhibitor Ku55933 partially rescues mitotic slippage caused by Nu7026 after 6 Gy. (Left) Analysis of senescent morphology in MFC7 cells treated with DMSO, Nu7026 (3 μM), Ku55933 (0.3 μM) or the combination for 1 h before 6 Gy and tracked by time-lapse recording. More than 50 cells from 10 randomly captured, non-overlapping images, were tracked for 4 d after irradiation. Cells with senescent morphology were classified as mono- or binucleated. Histogram shows mean ± s.d. **E.** SA-βGal staining in MCF7 cells. MCF7 control (Ctrl) or p21^{CIPI} overexpression (p21) cells were treated with DMSO, Aurora B inhibitor or PLK-1 inhibitor and stained after 4 d. At least 5 images were captured from randomly selected, non-overlapping fields. Representative images are shown. Mean percentage of SA-βGal$^+$ cells ± s.d. from five 20x fields indicated. Scale bar = 200 μm. **F.** Time-lapse analysis of MCF7-FUCCI cells treated with DMSO, Aurora B inhibitor (Aurora B i) or PLK-1 inhibitor (PLK-1 i). Representative cells shown at indicated times. Carets indicate cells that performed mitosis and cytokinesis during the time course. Scale bar = 50 μm. **G.** Analysis of senescent morphology in MCF7 cells treated as in **F**. More than 50 cells from 10 randomly captured, non-overlapping images, were tracked to 5 d after irradiation. Cells with senescent morphology were classified as mono- or binucleated. Histogram shows mean ± s.d. for each condition. **H**, Automated proliferation analysis from time-lapse imaging over 6 d comparing control (Ctrl) or p21^{CIPI} overexpression (p21) cells treated with DMSO, Aurora B inhibitor or PLK-1 inhibitor. For statistical analysis, unpaired t-test, **, $p < 0.01$; ***, $p < 0.001$. (Right) Diagram represents mononucleated or binucleated senescent cells. Scale bar = 50 μm.

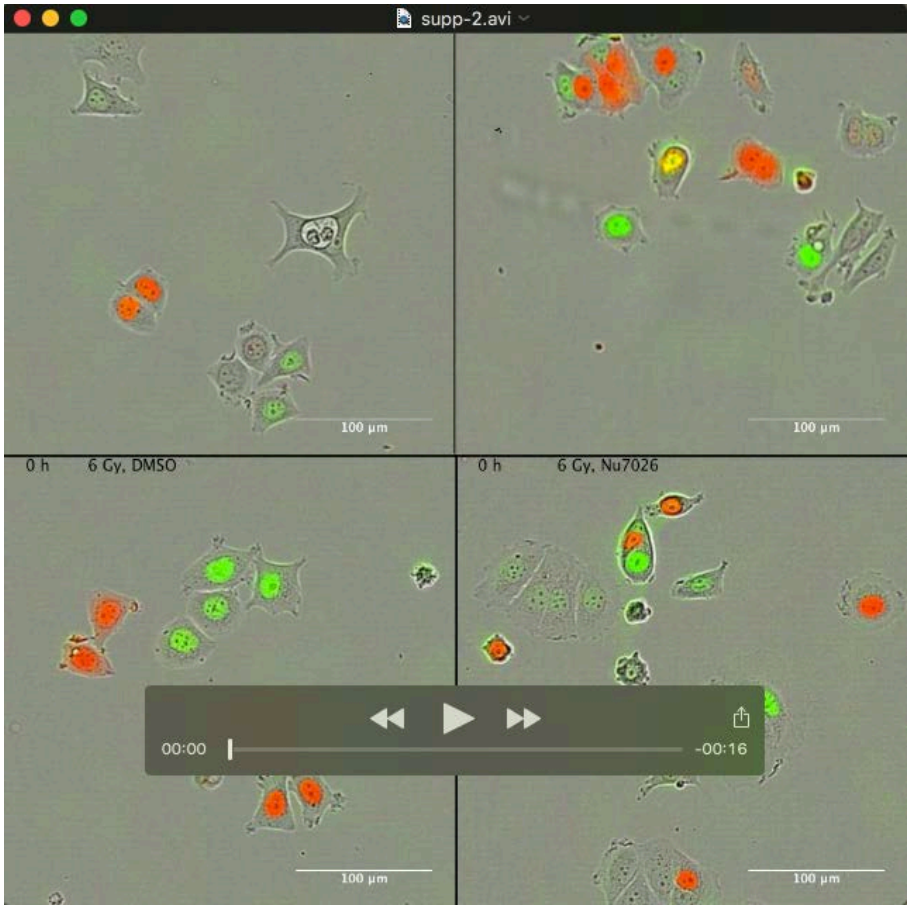

Movie 1. DNA-PKcs inhibitor Nu7026 induces mitotic slippage after irradiation, related to Figure 7 and Figure S5.

Time-lapse imaging of MCF7-FUCCI cells treated with DMSO or Nu7026 (3 µM) following 6 Gy irradiation or not. Cells were treated with DMSO or Nu7026 (3 µM) for 1 h, irradiated with 0 Gy or 6 Gy and then images were taken at 2 h intervals. Following 0 Gy, most of the cells underwent normal mitosis in which parent cells divided into two separated daughter cells approximately every 24 h in the presence or absence of Nu7026. Following 6 Gy, though some of the surviving cells treated with DMSO recovered from irradiation after a few cell cycles, others lost the capability for cell division and accumulate as flattened and enlarged cells displaying characteristic senescent morphology. However, many surviving cells with Nu7026 treatment entered the cell cycle but failed to complete cytokinesis and yielded binucleated cells, which adopted a senescent phenotype over time. Most cells with senescent morphology terminally arrested while expressing mCherry-hCdt1 (red), representing G1 cell cycle stage. Scale bar = 100 µm.

Journal of Cell Science • Supplementary information

Movie 2. ATM inhibitor Ku55933 partially rescues mitotic slippage caused by Nu7026 after 6 Gy, related to Figure 7 and Figure S6.

Time-lapse imaging of MCF7-FUCCI cells treated with Ku55933 (0.3 µM) or the combination of Ku55933 and Nu7026 (3 µM) following 6 Gy. Cells were treated with inhibitors for 1 h, irradiated with 6 Gy and then images were taken at 2 h intervals. In both cases, most surviving cells entered the cell cycle and completed cytokinesis, but many did not progress further. A high proportion of these daughters contained micronuclei and died instead of continuing on to senescence. Scale bar = 100 µm.

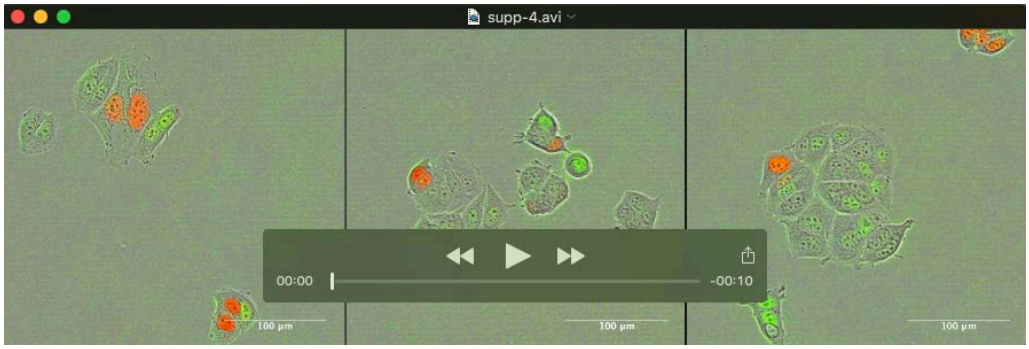

Movie 3. Mitosis and/or cytokinesis defects in unirradiated cells is sufficient to promote accelerated senescence, related to Figure 7 and Figure S7.

Time-lapse imaging of MCF7-FUCCI cells treated with DMSO, Aurora B kinase inhibitor, or PLK-1 inhibitor. Images were taken at 2 h intervals beginning 1 h after inhibitors treatment. With DMSO treatment, most of the cells underwent normal mitosis in which cell divided approximately every 24 h. With Aurora B kinase or PLK-1 inhibitor treatment, cells underwent mitotic slippage and/or catastrophe. Though many cells died, surviving cells eventually displayed senescent phenotype with mCherry-hCdt1 (red, G1) expression. Scale bar = 100 µm.

Movie 4. Overexpression of p21^{CIP1}rescues cell death induced by Aurora B or PLK1 inhibitors and yields homogeneous senescence, related to Figure 7 and Figure S7.

Time-lapse imaging of MCF7-FUCCI or p21^{CIPI} overexpression (p21) cells treated with DMSO, Aurora B or PLK1 inhibitors. Images were taken at 2 h intervals beginning 1 h after inhibitors treatment. In MCF7 cells with DMSO treatment, most of cells underwent cell cycle every 24 h. In MCF7 cells treated with Aurora B or PLK1 inhibitors, cells displayed mitotic slippage and some cells developed senescent morphology while some binucleate cells died rather than entering senescence. P21 overexpression can induce senescence on its own but when combined with the Aurora B or PLK1 inhibitors, the binucleate cells were rescued from death, yielding nearly homogeneous senescence.

Journal of Cell Science • Supplementary information

Table S1. List of chemical probes and their working concentrations.

Chemical probe	Targeted protein	Company	Catalog #	Working concentration
Nu7026	DNA-PKcs	Selleckchem	S2893	10 μM
Ku55933	ATM	Selleckchem	S1092	5 μM
CHIR124	Chk1	Cayman	16553	0.5 μM
Chk2 inhibitor	Chk2	Cayman	17552	5 μM
MK-8745	Aurora A	MedChem Express	HY-13819	1 μM
AZD1152-HQPA	Aurora B	MedChem Express	10126	0.5 μM
GSK461364	PLK-1	MedChem Express	50877	0.5 μM

Table S2. List of shRNAs.

Targeted protein	Sigma MISSION shRNA Catalog #	shRNA sequence
DNA-PKcs (PRKDC)(a)	TRCN0000195491	CCGGCCTCCAGGTTAGGATTAATTGCTCGAGCAATTAATCCTAACC TGGAGGTTTTTTG
DNA-PKcs (PRKDC)(b)	TRCN0000194719	CCGGCCTGAAGTCTTTACAACATATCTCGAGATATGTTGTAAAGAC TTCAGGTTTTTTG
ATM(a)	TRCN0000039948	CCGGCCTTTCATTCAGCCTTTAGAACTCGAGTTCTAAAGGCTGAAT GAAAGGTTTTTG
ATM (b)	TRCN0000039951	CCGGGCCTCCAATTCTTCACAGTAACTCGAGTTACTGGAAGAATTG GAGGTTTTTG
XRCC4 (a)	TRCN0000040117	CCGGCCTCAGGAGAATCAGCTTCAACTCGAGTTGAAGCTGATTCT C CTGAGGTTTTTG
XRCC4 (b)	TRCN0000009875	CCGGTGTGTGAGTGCTAAGGAAGCTCTCGAGAGCTTCCTTAGCAC T CACACATTTTTG
XRCC5(a)	TRCN0000295856	CCGGAGAGGAAGCCTCTGGAAGTTCCTCGAGGAACTTCCAGAGG C TTCCTCTTTTTTG
XRCC5(b)	TRCN0000307986	CCGGAATCTAAGAGAGCTGCCATCGCTCGAGCGATGGCAGCTCT C TTAGATTTTTTTG
XRCC6 (a)	TRCN0000039608	CCGGCGACATAAGTCGAGGGACTTTCTCGAGAAAGTCCCTCGAC T TATGTCGTTTTTG
XLF (a)	TRCN0000275632	CCGGTACCATGGACTTTAGGTATATCTCGAGATATACCTAAAGTCC ATGGTATTTTTG
XLF (b)	TRCN0000275628	CCGGGCTAGCAACGTTACTTCATATCTCGAGATATGAAGTAACGTT GCTAGCTTTTTG
PAXX(C9orf142)(a)	TRCN0000263653	CCGGCTCTTCTTACCAGACCCAGATCTCGAGATCTGGGTCTGGTA A GAAGAGTTTTTG
PAXX(C9orf142)(b)	TRCN0000263654	CCGGACAGAGCATCCCTGACGCTTTCTCGAGAAAGCGTCAGGGA T GCTCTGTTTTTTG
Ligase4(a)	TRCN0000040004	CCGGGCCCGTGAATATGATTGCTATCTCGAGATAGCAATCATATTC ACGGGCTTTTTG
Ligase4(b)	TRCN0000040005	CCGGGCTCGCATCTAAACACCTTTACTCGAGTAAAGGTGTTTAGAT GCGAGCTTTTTG
RNF144A(a)	TRCN0000004413	CCGGGAACGAGATTGAGTGCATGGTCTCGAGACCATGCACTCAA T CTCGTTCTTTTT
RNF144A(b)	TRCN0000421486	CCGGATGTTGAGCTCTTGATCAAAGCTCGAGCTTTGATCAAGAGC T CAACATTTTTTTG
XRCC1(a)	TRCN0000007912	CCGGCCTTCTGGTCACCTCATCTTTCTCGAGAAAGATGAGGTGACC A GAAGGTTTTT
XRCC1(b)	TRCN0000007913	CCGGCCAGTGCTCCAGGAAGATATACTCGAGTATATCTTCCTGGAG C ACTGGTTTTT
Ligase3(a)	TRCN0000048499	CCGGCCGGATCATGTTCTCAGAAATCTCGAGATTTCTGAGAACATGA TCCGGTTTTTG
Ligase3(b)	TRCN0000048500	CCGGGCTGAGTAACTCCAACAGCAACTCGAGTTGCTGTTGGAGTT A CTCAGCTTTTTG

Table S3. List of antibodies.

Antibody/protein	Company	Catalog #	Dilution
γ-H2AX, clone JBW301	EMD Millipore	05-636	1:1000
γ-H2AX(Alexa 647 conjugate)	Cell Signaling Technology	9720	1:50
γ-H2AX	Cell Signaling Technology	9718	1:1000
53BP1	Novus	NB100-304	1:1000
DNA-PKcs	Abcam	ab32566	1:500
DNA-PKcs	Cell Signaling Technology	12311	1:1000
DNA-PKcs (Phospho T2609)	Abcam	ab97611	1:500
DNA-PKcs (Phospho S2056)	Abcam	ab124918	1:1000
ATM	Abcam	ab78	1:200
ATM	Cell Signaling Technology	2873	1:1000
ATM (Phospho S1981)	Cell Signaling Technology	4526	1:1000
XRCC5	Abcam	ab80592	1:1000
Ku80	Cell Signaling Technology	2180	1:1000
XRCC6	Abcam	ab202022	1:1000
XRCC4	Abcam	ab97351	1:1000
PAXX	Abcam	ab126353	1:1000
XLF	Abcam	ab33499	1:1000
Ligase4	Abcam	ab26039	1:800
RNF144A	Abcam	ab89260	1:100
Actin (HRP conjugate)	Proteintech	HRP-60008	1:10000
Tubulin (HRP conjugate)	Proteintech	HRP-66031	1:10000